The Mitochondrial Permeability Transition Pore Activates the Mitochondrial Unfolded Protein Response and Promotes Aging

Suzanne Angeli[1*], Anna C. Foulger[1], Manish Chamoli[1], Tanuja Harshani Peiris[1], Akos A. Gerencser[1] Azar Asadi Shahmirzadi[1,2], Julie K. Andersen[1,2*], Gordon J. Lithgow[1,2*]

[1]Buck Institute for Research on Aging; Novato, California, 94945 USA
[2]USC Leonard Davis School of Gerontology, University of Southern California, Los Angeles, California, 90191

*Correspondence: sangeli@buckinstitute.org, glithgow@buckinstitute.org, jandersen@buckinstitute.org

SUMMARY

Mitochondrial activity determines aging rate and the onset of chronic diseases. The mitochondrial permeability transition pore (mPTP) is a pathological pore in the inner mitochondrial membrane thought to be composed of the F-ATP synthase (complex V). OSCP, a subunit of F-ATP synthase, helps protect against mPTP formation. How the destabilization of OSCP may contribute to aging, however, is unclear. We have found that loss OSCP in the nematode *Caenorhabditis elegans* initiates the mPTP and shortens lifespan specifically during adulthood, in part via initiation of the mitochondrial unfolded protein response (UPR^{mt}). Pharmacological or genetic inhibition of the mPTP inhibits the UPR^{mt} and restores normal lifespan. Loss of the putative pore-forming component of F-ATP synthase extends adult lifespan, suggesting that the mPTP normally promotes aging. Our findings reveal how an mPTP/UPR^{mt} nexus may contribute to aging and age-related diseases and how inhibition of the UPR^{mt} may be protective under certain conditions.

INTRODUCTION

As mitochondrial function declines with age, the frequency of the mPTP increases (Rottenberg and Hoek, 2017). The mPTP is central to early-stage pathologies associated with several age-related diseases, including Alzheimer's and Parkinson's disease (AD, PD) and late-stage pathologies of ischemia-reperfusion injuries including heart attack and stroke (Ong et al., 2015; Panel et al., 2018). The mPTP is a pathological channel that forms in the inner mitochondrial membrane in response to excessive cytosolic Ca^{2+} or high ROS conditions. Sustained opening of the mPTP leads to outer mitochondrial membrane rupture, release of Ca^{2+} into the cytosol, and cell death (Bernardi and Di Lisa, 2015). Cyclosporin A (CsA), a well-characterized mPTP inhibitor, inhibits the mPTP by binding and sequestering cyclophilin D, a mitochondrially-localized peptidyl prolyl isomerase that helps catalyze pore formation (Basso et al., 2005; Nakagawa et al., 2005). Genetic inhibition of cyclophilin D protects against mPTP formation (Baines et al., 2005) and CsA has been shown to extend lifespan in *C. elegans* (Ye et al., 2014). Thus, the mPTP appears to be an important modulator of healthspan and lifespan.

The identification of the proteins that make up the mPTP is controversial. Recent models have moved away from the models that invoked the voltage-dependent anion channel (VDAC), mitochondrial phosphate carrier (PiC), and translocator protein (TPSO) due to genetic ablation studies showing that the mPTP can still occur in their absence (Kwong and Molkentin, 2015).

Due to a multitude of recent studies, many experts in the field of mPTP have pointed to the F-ATP synthase (complex V) as the most probable inner mitochondrial pore candidate (Bonora et al., 2017; Carraro et al., 2019; Mnatsakanyan and Jonas, 2020). F-ATP synthase is able to bind cyclophilin D and form Ca^{2+} currents (Bernardi and Di Lisa, 2015; Mnatsakanyan and Jonas, 2020). Some models posit that dimeric forms of F-ATP synthase open to form a pore while other models have suggested that the pore occurs via the membrane-bound proton-driving c-ring rotor (Alavian et al., 2014; Azarashvili et al., 2014; Bonora et al., 2013; Bonora et al., 2017; Giorgio et al., 2013; Mnatsakanyan et al., 2019; Neginskaya et al., 2019; Urbani et al., 2019). Despite mounting evidence supporting F-ATP synthase as the pore-forming component of the mPTP, systematic deletion nearly every subunit of F-ATP synthase in a cell model showed that a pore is still capable of forming (Carroll et al., 2019; He et al., 2017a; He et al., 2017b), leading some groups to suggest that in the absence of an intact F-ATP synthase, smaller low conductance CsA-dependent pores distinct from the mPTP form (Neginskaya et al., 2019). Other groups have proposed that the mPTP can be mediated by adenine nucleotide transporter (ANT), which exchanges ADP and ATP across the IMM. Genetic inhibition of ANTs helps prevent pore formation (Karch et al., 2019), and the "multi-pore model" posits that the mPTP can be mediated by ANT, as well as a cyclophilin D binding structure, such as F-ATP synthase, which would explain why deletion of putative pore components may still yield pore formation (Carraro et al., 2019; Karch et al., 2019).

ATP5O, also known as oligomycin sensitivity-conferring protein (OSCP), a subunit of the F-ATP synthase that regulates ATPase rotational activity to provide efficient ATP production (Murphy et al., 2019), has emerged as an important regulator of the mPTP. OSCP confers protection against the mPTP under low pH conditions and loss of OSCP increases propensity for mPTP formation *in vitro* (Antoniel et al., 2018; Giorgio et al., 2013). In mice, levels of OSCP decrease with normal aging (Gauba et al., 2017). In mouse models of AD, OSCP binds to amyloid beta (Aβ) and the propensity for mPTP formation increases, suggesting that the destabilization of OSCP contributes to mPTP formation (Beck et al., 2016b). Conversely, OSCP overexpression protects from mPTP initiation in AD and cardiac dysfunction models (Beck et al., 2016b; Guo et al., 2020). Thus, OSCP appears to be an important regulator of aging and disease progression, possibly via its ability to modulate mPTP formation.

Under stress, the mitochondria attempt to repair the damage, recycle damaged mitochondria, or, under deleterious circumstances, initiate cell death. Similar to the endoplasmic reticulum unfolded protein response (UPR^{ER}) and the cytoplasmic heat shock response (HSR), the mitochondrial unfolded protein response (UPR^{mt}) is capable of initiating a broad-range transcriptional response that, among other functions, aids in the refolding of mitochondrial matrix proteins (Naresh and Haynes, 2019). Recent studies also show that a loss of mitochondrial membrane potential (MMP) correlates with activation of the UPR^{mt}, and disruption of mitochondrial processes other than protein misfolding, such as those involved in TCA cycle and lipid catabolism, also induce the UPR^{mt} (Rolland et al., 2019). UPR^{mt} activation is associated with longevity and improvement in neurodegenerative models (Durieux et al., 2011; Houtkooper et al., 2013; Kim et al., 2016; Merkwirth et al., 2016; Sorrentino et al., 2017; Tian et al., 2016), but it has also conversely been shown to increase neurodegeneration, propagate mtDNA mutations, and exacerbate ischemic conditions (Lin et al., 2016; Martinez et al., 2017; Yung et al., 2019), underscoring its complexity. If left unmitigated, UPRs can initiate cell death (Iurlaro

and Munoz-Pinedo, 2016; Munch and Harper, 2016). Thus, the context or cellular environment are important determinants of whether UPR^{mt} induction results in beneficial or detrimental effects.

In *C. elegans*, mild mitochondrial perturbations early in life can extend lifespan. Loss of OSCP/*atp-3* has previously been shown to extend lifespan when initiated during larval development (Dillin et al., 2002; Rea et al., 2007). In contrast, here, we have determined that loss of OSCP/*atp-3* during adulthood leads to initiation of the mPTP, the UPR^{mt}, and a shortened lifespan. Surprisingly, *atfs-1*, the UPR^{mt} master transcription factor (Haynes et al., 2010; Nargund et al., 2012), helps drive the reduction of lifespan, suggesting that the UPR^{mt} program can promote aging during adulthood. The adult UPR^{mt} is responsive to mPTP regulators, including the immunosuppressive drug, CsA, as well as a mitochondrially-localized cyclophilin and ANTs, pointing to a previously undiscovered coordination between the UPR^{mt} and the mPTP. We find that proton-driving rotor subunits as well as subunits important for dimerization of the F-ATP synthase are essential for transducing the adult UPR^{mt}. Loss of these subunits as well as pharmacological CsA treatment restores lifespan due to loss of OSCP/*atp-3*. These results are consistent with current models that posit that the F-ATP synthase forms the mPTP (Bernardi and Di Lisa, 2015). Overall, our findings point to a model in which loss of OSCP/*atp-3* in adults induces mPTP formation and subsequent detrimental activation of the UPR^{mt}. Understanding the relationship between these two mitochondrial processes will further our understanding of aging as well as disparate age-related disorders, including neurodegenerative diseases, cancer, heart-attack, and stroke.

RESULTS

Loss of OSCP/*atp-3* Induces Mitochondrial Permeability Transition Pore (mPTP) Characteristics During Adulthood

The opening of the mPTP is characterized by a loss of mitochondrial membrane potential (MMP) as well as an increase in cytosolic Ca^{2+} and responsiveness to the mPTP inhibitor, CsA. We observed that a reduction in the abundance of OSCP/*atp-3* by RNA interference (RNAi) during adulthood caused a loss of MMP as measured by the mitochondrial dye, TMRM, while RNAi of other OXPHOS subunits from complex I, IV, and V had no effect on the MMP (Figures 1A, B). RNAi of OSCP/*atp-3* during adulthood also caused an increase in cytosolic Ca^{2+} as measured by the intestinal FRET-based Ca^{2+} reporter, KWN190, while RNAi of subunits from complex IV and complex V did not (Figures 1D, E). CsA rescued the loss of MMP and suppressed the rise of cytosolic Ca^{2+} caused by RNAi of OSCP/*atp-3* during adulthood (Figures 1C, F). Loss of OSCP/*atp-3* also induced mitochondrial swelling and fragmentation compared to control, which was rescued by CsA (Figures 1G-J). To determine if a loss of MMP during adulthood was sufficient to recapitulate mPTP characteristics, we tested the effects of FCCP, a potent mitochondrial uncoupler. FCCP induced a loss of MMP when administered during adulthood, but did not lead to an increase in cytosolic Ca^{2+} (Figure 1- figure supplement 1A, B), suggesting that a loss in MMP is not sufficient to recapitulate mPTP characteristics. Similarly, loss of OSCP/*atp-3* RNAi during development, which leads to a loss of MMP, did not lead to an increase in cytosolic Ca^{2+} (Figure 1- figure supplement 1C, D), demonstrating that phenotypes that result from a loss of OSCP/*atp-3* are distinct during adulthood versus development. Overall, these results suggest that loss of OSCP/*atp-3* during adulthood uniquely induces the mPTP in *C. elegans*.

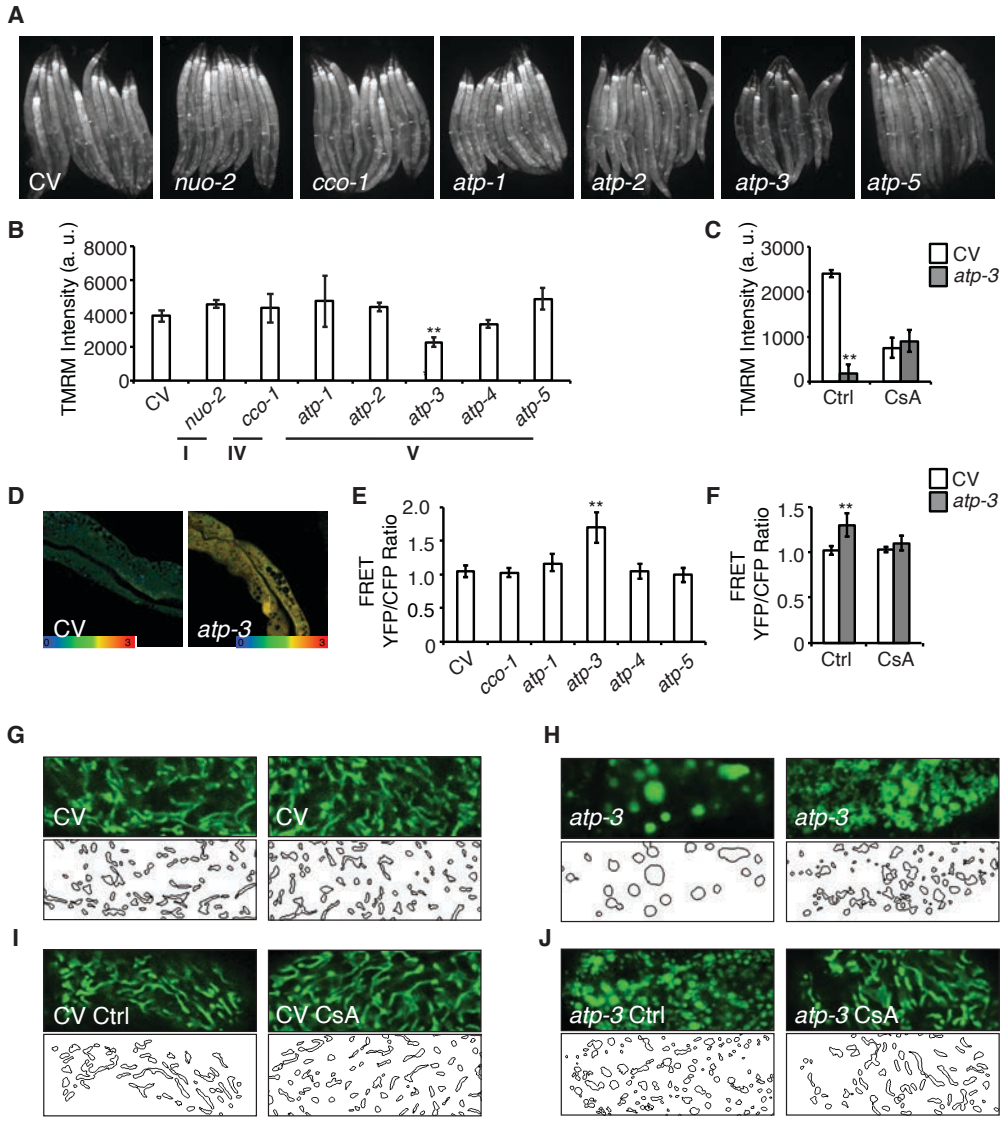

Figure 1: Loss of OSCP/*atp-3* Selectively Recapitulates mPTP-like Characteristics During Adulthood.
(A) Photomicrographs of MMP as measured by TMRM after RNAi of OXPHOS subunits. RNAi and TMRM were administered for 48 hours beginning at young adulthood. Representative micrographs shown.
(B) Quantification of TMRM intensity from (A). Data are the mean ± SEM of ≤ 15 animals combined from three biological experiments. **p ≤ 0.01 by Student's *t*-test. I, IV, and V correspond to OXPHOS complexes. a. u., arbitrary units.
(C) Quantification of MMP after RNAi of OSCP/*atp-3* and treatment with CsA (15 μM). RNAi and CsA were administered beginning at young adulthood for 24 hours. Data are the mean ± SEM of ≤ 15 animals combined from three biological experiments. *p ≤ .05, **p ≤ .01 by Student's *t*-test. a. u., arbitrary units.
(D) Confocal micrograph of intestinal cytosolic Ca^{2+} as measured by the FRET-based calcium indicator protein D3cpv/cameleon after OSCP/*atp-3* RNAi. RNAi was administered for 48 hours beginning at young adulthood. Representative micrograph shown.
(E) Quantification of FRET YFP/CFP ratio after RNAi of OXPHOS subunits. RNAi was administered for 48 hours beginning at young adulthood. Data are the mean ± SEM of ≤ 15 animals combined from three biological experiments. **p ≤ .01 by Student's *t*-test.
(F) Quantification of FRET YFP/CFP ratio after RNAi of OSCP/*atp-3* and treatment with CsA (15 μM). RNAi and CsA were administered beginning at young adulthood for 48 hours. Data are the mean ± SEM of ≤ 15 animals combined from three biological experiments. **p ≤ .01 by Student's *t*-test.
(G-J) Confocal micrographs of intestinal mitochondria labeled with GFP (p*ges-1*::GFP^{mt}) in young adults. RNAi and CsA was administered for 48 hours beginning at young adulthood, then worms were removed from the RNAi and CsA and aged until Day 7 of adulthood followed by collection for microscopy. Top panels, fluorescent channel; bottom panels, rendering of individual mitochondria. CV, control vector, Ctrl, solvent control, CsA, 15 μM. See Materials and Methods for details on rendering.

To determine if RNA expression levels of OSCP/*atp-3* may be higher during adulthood compared to other OXPHOS subunits, which would sensitize it to RNAi, we examined available RNAseq data from *wormbase.org*. Fragments per kilobase of transcript per million (FPKM) expression values of various OXPHOS subunits collected at young adulthood (YA) showed that OSCP/*atp-3* did not display higher expression compared to other subunits, and that its expression during larval stages (L1) and YA were also comparable (Figure 1- figure supplement 1G). To verify that the lack of a phenotypes from the other OXPHOS subunits was not due to inefficient RNAi, we checked for RNAi efficiency via qPCR. We observed efficient mRNA reduction for all tested subunits, suggesting that the RNAi was effective (Figure 1- figure supplement 1E). We also examined protein levels for subunits in which antibodies were available and observed that RNAi of the complex I subunit NUO-2 and complex V subunits ATP-1 and ATP-2 resulted in significant knockdown of protein levels (Figure 1- figure supplement 1F). These findings support our conclusions that loss of OSCP/*atp-3* uniquely recapitulates mPTP characteristics during adulthood.

Loss of OSCP/*atp-3* Induces a Unique UPR^{mt} During Adulthood

A recent study showed that a loss of MMP in *C. elegans* during development is associated with induction of the UPR^{mt} (Rolland et al., 2019). To determine if RNAi of OSCP/*atp-3* selectively induces the UPR^{mt} during adulthood due to its observed loss in MMP (Figures 1A, 1B), we utilized a GFP reporter under the promoter of the UPR^{mt} chaperone, *hsp-6* (p*hsp-6*::GFP) (Yoneda et al., 2004) and compared it to select representative OXPHOS genes encoding complex I, III, IV, and V subunits. RNAi of OXPHOS subunits induced little to no UPR^{mt} if initiated after the last larval stage (L4), which we termed the post-developmental UPR^{mt} (pdvUPR^{mt}) (Figures 2A, B and Figure 2- table supplement 1). The exception was RNAi of OSCP/*atp-3*, which induced a robust UPR^{mt} in young adults (Figures 2A, B and Figure 2- table supplement 1), the timing of which corresponded with the loss in MMP (Figures 1A, B). In contrast, RNAi of all the same genes induced a robust UPR^{mt} if initiated during the early larval stages (L1, L2, and L3) of development (dvUPR^{mt}) (Figures 2A, B). These results are consistent with previous reports demonstrating that the UPR^{mt} is robustly induced during development but poorly induced during adulthood in *C. elegans* (Durieux et al., 2011; Labbadia and Morimoto, 2015). Treating worms with FCCP during adulthood did not induce the UPR^{mt} (Figure 2- figure supplement 2A), indicating that loss of MMP per se is not sufficient to induce the UPR^{mt} during adulthood. Post-developmental loss of OSCP/*atp-3* increased endogenous transcript levels of *hsp-6* as well as endogenous HSP-6/mtHSP70 protein levels (Figure 2- figure supplement 2B, C). Post-developmental loss of OSCP/*atp-3* mildly induced the mitochondrial chaperone reporter p*hsp-60::*GFP (Figure 2- figure supplement 2D, E). Neither the UPR^{ER} nor the HSR were induced by post-developmental loss of OSCP/*atp-3* (Figure 2- figure supplement 2E). RNAi of other mitochondrial genes that are known to induce a dvUPR^{mt}, *clk-1* (coenzyme Q hydroxylase), *mrps-5* (mitochondrial ribosome), and *tomm-22* (translocase of outer mitochondrial membrane) (Baker et al., 2012; Bennett et al., 2014; Houtkooper et al., 2013), did not induce the pdvUPR^{mt} (Figure 2- table supplement 1). Importantly, we found that the pdvUPR^{mt} was dependent on the master UPR^{mt} transcription factor, *atfs-1* (Figure 2C) (Haynes et al., 2010), demonstrating that the pdvUPR^{mt} is regulated similarly to the previously described dvUPR^{mt}. Thus, loss of OSCP/*atp-3* induces a robust and specific pdvUPR^{mt} which is dependent on the conserved transcription factor ATFS-1.

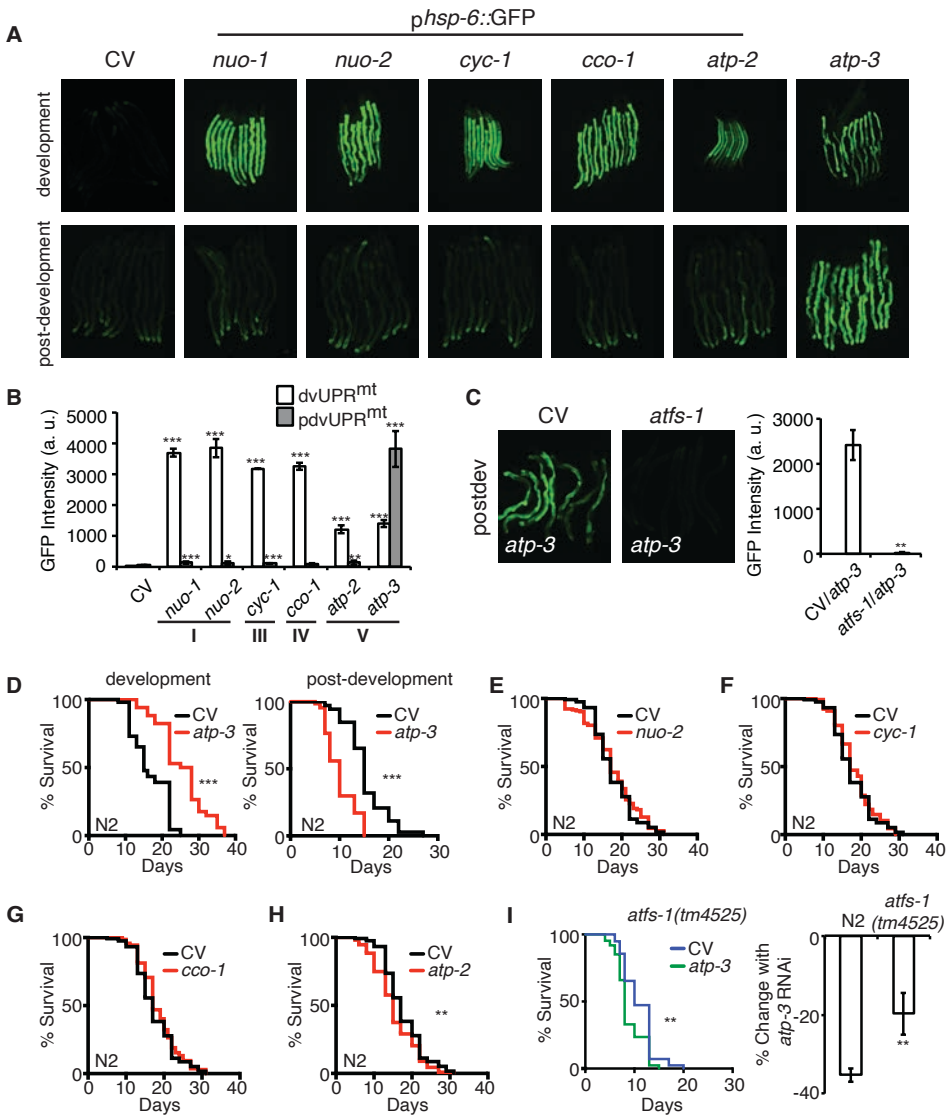

Figure 2: Loss of OSCP/*atp-3* Initiates a Unique UPR^{mt} and Shortens Lifespan During Adulthood

(A) Photomicrographs of p*hsp-6*::GFP reporter after developmental or post-developmental RNAi of OXPHOS subunits. For developmental treatment, worms were exposed to RNAi beginning from eggs for 72 hours. For post-developmental treatment, worms were exposed to RNAi beginning from young adulthood for 48 hours. CV, control vector; dev, development; post-dev, post-development.

(B) Quantification of GFP intensity from (A). Data are the mean ± SEM of ≤ 15 animals combined from three biological experiments. *p ≤ 0.05, **p ≤ 0.01, and ***p ≤ .0001 by Student's *t*-test. dv, development; pdv, post-development; I, III, IV, and V refer to OXPHOS complexes.

(C) Photomicrographs of the p*hsp-6*::GFP reporter after RNAi of OSCP/*atp-3* and *atfs-1*. Worms were exposed to RNAi beginning from young adulthood for 48 hours. Bar graph represents quantification of GFP intensity. Data are the mean ± SEM of ≤ 15 animals combined from three biological experiments. **p ≤ 0.01 by Student's *t*-test. CV, control vector RNAi; pdv, post-development.

(D) Survival curves of wild-type N2 animals on CV or OSCP/*atp-3* RNAi. For developmental RNAi, worms were treated continuously since eggs. For post-developmental RNAi, worms were treated for 48 hours beginning at young adulthood. Representative curves selected from three biological experiments. ***p ≤ .0001 by Log Rank (Mantel Cox). CV, control vector.

(E-H) Survival curves of wild-type N2 animals on indicated RNAi initiated at young adulthood for 48 hours. Representative curves selected from three biological experiments. **p ≤ 0.01 by Log Rank (Mantel Cox).

(I) Survival curves of *atfs-1(tm4525)* when OSCP/*atp-3* RNAi is initiated at young adulthood for 48 hours. Representative curves selected from three biological experiments. **p ≤ 0.01 by Log Rank (Mantel Cox). Bar graph is a quantification of percent change in lifespan of N2 or *atfs-1(tm4525)* mutant. **p ≤ 0.01 by Student's *t*-test is the mean of the percent change in lifespan ± SEM from three biological experiments. CV, control vector RNAi.

Loss of OSCP/*atp-3* During Adulthood Shortens Lifespan
Previous reports have shown that loss of OSCP/*atp-3* initiated during development robustly increases lifespan in *C. elegans* (Dillin et al., 2002), but how loss of OXPHOS subunits during adulthood affects lifespan has not been well studied. We initiated OSCP/*atp-3* RNAi during both development and post-development. As previously reported, we found that continuous RNAi treatment initiated during development (beginning from eggs) led to lifespan extension (Figure 2D and Source Data 1). Worms continuously exposed to OSCP/*atp-3* RNAi during post-development experienced a high incidence of matricide (data not shown). To circumvent this outcome, we administered OSCP/*atp-3* RNAi to young adults for 48 hours of adulthood and observed approximately a 38% decrease in lifespan independent of matricide (Figure 2D and Source Data 1). Loss of other OXPHOS subunits had little or no effect on lifespan when administered during adulthood for 48 hours (Figures 2E-H, Suppl. Table 4). Surprisingly, when putative null *atfs-1(tm4525)* mutants were exposed to OSCP/*atp-3* RNAi during adulthood for 48 hours, we observed only about a 19% decrease in lifespan, suggesting that the initiation of the pdvUPR^{mt} via *atfs-1* contributes to reduced lifespan (Figure 2I and Source Data 1). Thus, we have identified that loss of OSCP/*atp-3* has distinct effects in lifespan depending on if RNAi is initiated during adulthood versus development, which has not been previously described in *C. elegans.*

To further probe the developmental versus post-developmental effects on longevity from the loss of OSCP/*atp-3*, we tested how post-developmental RNAi of OSCP/*atp-3* would affect the longevity of worms treated with COX5B/*cco-1* RNAi during development, which has been shown to be sufficient to extend lifespan ((Durieux et al., 2011). Developmental treatment with COX5B/*cco-1* RNAi followed by post- developmental treatment with OSCP/*atp-3* RNAi did not significantly alter the long-lived lifespan (Figure 2- figure supplement 2F and Source Data 1), suggesting that the effects of developmental COX5B/*cco-1* RNAi override the post-developmental effects of OSCP/*atp-3* RNAi, potentially due to the epigenetic remodeling that occurs during development (Merkwirth et al., 2016).

The Post-Developmental UPR^{mt} is Temporally Confined and Reversible
Given that the UPR^{mt} has not been studied during adulthood in *C. elegans,* we sought to determine the window of the UPR^{mt} during adulthood. We initiated RNAi of OSCP/*atp-3* beginning at the last larval stage (L4 stage) and every few hours thereafter into adulthood. GFP expression was examined 48 hours after RNAi initiation (Figure 2- figure supplement 3A). We observed that the pdvUPR^{mt} was initiated up to 6 hours after the L4 stage, after which RNAi of OSCP/*atp-3* no longer induced the UPR^{mt}. In contrast, RNAi of COX5B/*cco-1* of complex IV had no effects on the UPR^{mt} at any of these stages (Figure 2- figure supplement 3A). For all subsequent post-development experiments, RNAi was therefore administered at the young adult stage corresponding to 4-hours after the L4 stage. Thus, the pdvUPR^{mt} is confined to pre-gravid stages of adulthood, corresponding with previous reports showing a global decline in stress responses at the onset of egg-laying (Labbadia and Morimoto, 2015).

Previous studies have shown that developmental RNAi of COX5B/*cco-1* RNAi leads to persistent activation of the UPR^{mt} into adulthood, even after removal from RNAi (Durieux et al., 2011). Similarly, we observed that developmental RNAi of OSCP/*atp-3* initiated a UPR^{mt} that persisted into adulthood, even after removal from OSCP/*atp-3* RNAi (Figure 2- figure

supplement 3B). In contrast, removal from post-developmental OSCP/*atp-3* RNAi treatment led to a steady decline in the GFP signal (Figure 2- figure supplement 3B), suggesting the activation of the pdvUPR^{mt} is reversible.

The Post-Developmental UPR^{mt} is Dependent on Mitochondrial Permeability Transition Pore (mPTP) Factors

To determine if the pdvUPR^{mt} is initiated in response to the mPTP, we tested pharmacological and genetic modulators of the mPTP on induction of the pdvUPR^{mt}. CsA binds cyclophilins, which in the cytoplasm regulates calcineurin signaling (Liu et al., 1991; Takahashi et al., 1989), while in the mitochondria inhibits the mPTP (Nicolli et al., 1996). To parse out the mitochondrial versus cytoplasmic functions of CsA, we also tested the cytoplasmic-only immunosuppressive drug, FK506, which acts similarly to CsA in that it modulates calcineurin signaling in the cytoplasm (Liu et al., 1991). We observed that CsA strongly inhibited the pdvUPR^{mt} but not dvUPR^{mt} in a dose-dependent manner (Figures 3A, C and Figure 3-figure supplement 4A). In contrast, we found that FK506 had no effect on the pdvUPR^{mt} (Figures 3A, C, and Figure 3-figure supplement 4B), demonstrating that CsA acts in the mitochondria to suppress the pdvUPR^{mt}. The mPTP has been shown to be regulated by adenine nucleotide translocases (ANTs) of the inner mitochondrial membrane and loss of ANTs helps prevent the mPTP (Karch et al., 2019). We tested *ant-1.1*, which is ubiquitously expressed in *C. elegans*, and *ant-1.2*, which is expressed predominantly in the pharynx and intestines (Farina et al., 2008). RNAi of

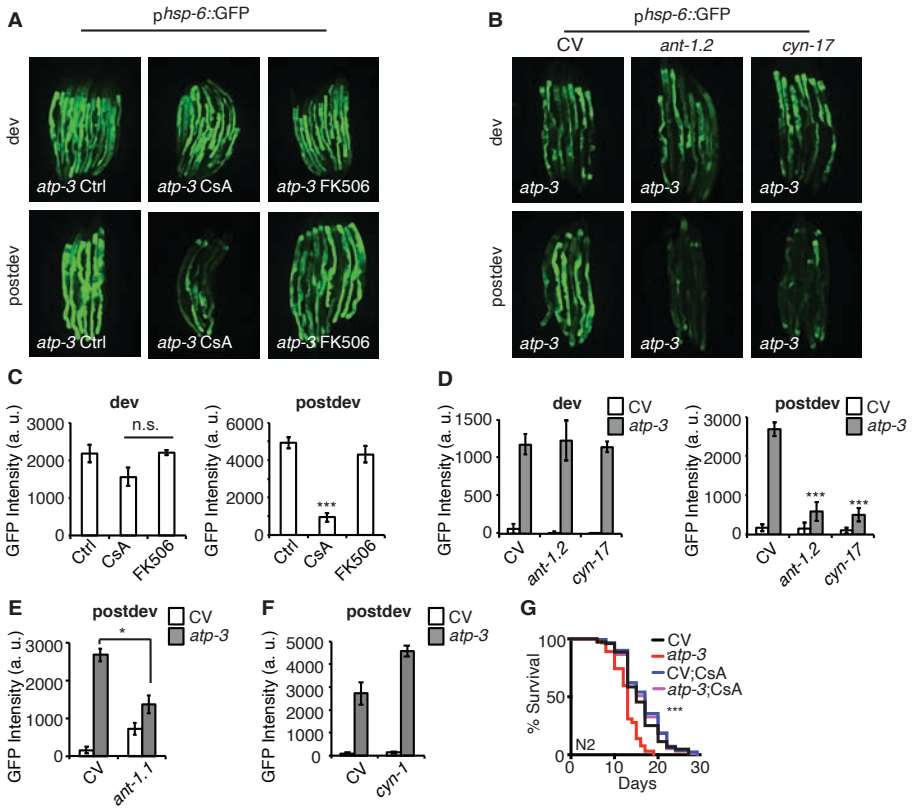

Figure 3: The Post-Developmental UPR^{mt} is Regulated by Pharmacological and Genetic Modulators of the mPTP

(A, B) Photomicrographs of p*hsp-6*::GFP reporter after developmental or post-developmental RNAi an drug treatments (CsA and FK506, 15 µM). For developmental treatment, worms were treated beginning from eggs for 72 hours. For post-developmental treatment, worms were treated beginning from young adulthood for 48 hours. dev, development; post-dev, post-development.
(C, D) Quantification of GFP intensity from (A, B). Data are the mean ± SEM of ≤ 15 animals combined from three biological experiments. *p ≤ .05,***p ≤ .0001 by Student's *t*-test; n. s., not significant; CV, control vector, dev, development; post-dev, post-development.
(E, F) Quantification of GFP intensity from p*hsp-6*::GFP reporter after RNAi treatment for 48 hours beginning from young adulthood. CV, control vector, post-dev, post-development.
(G) Survival curves of wild-type N2 animals on CV or OSCP/*atp-3* RNAi with either solvent control or CsA (15 µM). RNAi and CsA were administered beginning at young adulthood for 48 hours and then transferred to regular NGM plates for the remainder of the lifespan. Representative curves selected from three biological experiments. ***p ≤ .0001 by Log Rank (Mantel Cox). CV, control vector.

ant-1.1 moderately suppressed the pdvUPR^{mt} (Figure 3E) while RNAi of *ant-1.2* strongly suppressed the pdvUPR^{mt}, but not the dvUPR^{mt} (Figures 3B, D). In mammals, CsA acts in the mitochondria to inhibit the mPTP by binding and sequestering cyclophilin D, a peptidyl prolyl isomerase (Nicolli et al., 1996). *C. elegans* contains 17 poorly defined cyclophilins, of which 2 are predicted to be mitochondrially localized, *cyn-1* and *cyn-17* (Figure 3- table supplement 2). RNAi of *cyn-1* did not inhibit the pdvUPR^{mt} (Figure 3F) while *cyn-17* did (Figure 3B, D), suggesting that *cyn-17* may act similarly to cyclophilin D in mediating a conformation change that leads to the mPTP. RNAi of *cyn-17* did not affect the dvUPR^{mt} (Figures 3B, D). Finally, we observed that CysA was able to reverse the lifespan shortening caused by OSCP/*atp-3* RNAi (Figure 3G), demonstrating that inhibition of the UPR^{mt} can be beneficial under certain conditions. Together, these results show that the pdvUPR^{mt} is regulated by canonical pharmacological and genetic mPTP factors.

Loss of F-ATP Synthase ATPases Induce a Post-Developmental UPR^{mt}

F-ATP synthase is composed of a membrane-bound proton-driving rotor (Fo), a catalytic ATPase that converts ADP to ATP (F1), and peripheral stalk and supernumerary subunits that help bridge these two portions together (Figure 4E). OSCP/*atp*-3 sits on the ATPase and helps tether it to the peripheral stalk subunits. We systematically tested via RNAi whether loss of F-ATP synthase subunits other than OSCP/*atp-3* could induce a pdvUPR^{mt}. During development, loss of rotor subunits, ATPase subunits, or peripheral stalk and supernumerary subunits all induced a robust UPR^{mt} (Figure 4A, C). In contrast, during adulthood, loss of rotor subunits (c-ring/*Y82E9BR.3*), peripheral stalk or supernumerary subunits (F6/*atp-4*, d/*atp-5*, b/*asb-2*, e/*R04F11.2*, f/*R53.4*), induced little to no UPR^{mt} (Figure 4B, D and Figure 4- table supplement 3). Loss of the ATPase subunits (α/*atp-1*, β/*atp-2*, δ/*F58F12.1*, ε/*hpo-18*) induced a mild to moderate UPR^{mt}, though none as robustly as loss of OSCP/*atp-3*. We observed that post-developmental loss of the α/*atp-1* ATPase subunit exhibited the second most robust pdvUPR^{mt} (Figure 4B, D) but did not induce a loss of MMP or a rise in cytosolic Ca^{2+} (Figures 1A-C). Consistently, we observed a minor shortening of survival due to post-developmental RNAi of α/*atp-1* (Figure 4F). These findings support our hypothesis that loss of OSCP/*atp-3*, but not other F-ATP synthase subunits, activates an mPTP that is coupled to a maladaptive pdvUPR^{mt}.

Loss of F-ATP Synthase Subunits Important for the Formation of the mPTP Suppress the Post-Developmental UPR^{mt}

Current models posit that the F-ATP synthase forms a pore that is capable of releasing Ca^{2+} under conditions of high oxidative stress, leading to rupturing of the mitochondria and initiation of cell death cascades. Some models suggest that F-ATP synthase dimers form the mPTP (Figure 5E) and that peripheral and supernumerary subunits are essential for pore formation (Carraro et al., 2014; Giorgio et al., 2013; Guo et al., 2019; Urbani et al., 2019). Other models demonstrate that F-ATP synthase monomers are sufficient for the mPTP and specify the c-ring proton-driving rotor as the actual pore-forming component (Figure 5F) (Alavian et al., 2014; Azarashvili et al., 2014; Bonora et al., 2013; Bonora et al., 2017; Mnatsakanyan et al., 2019; Neginskaya et al., 2019). To determine whether the structural integrity of F-ATP synthase subunits was required for the pdvUPR^{mt}, we systematically knocked down OSCP/*atp-3* as well as one additional F-ATP synthase subunit via RNAi. When we knocked down the c-ring subunits (color coded black) as well as peripheral and supernumerary subunits (color coded grey) via RNAi in adults, we

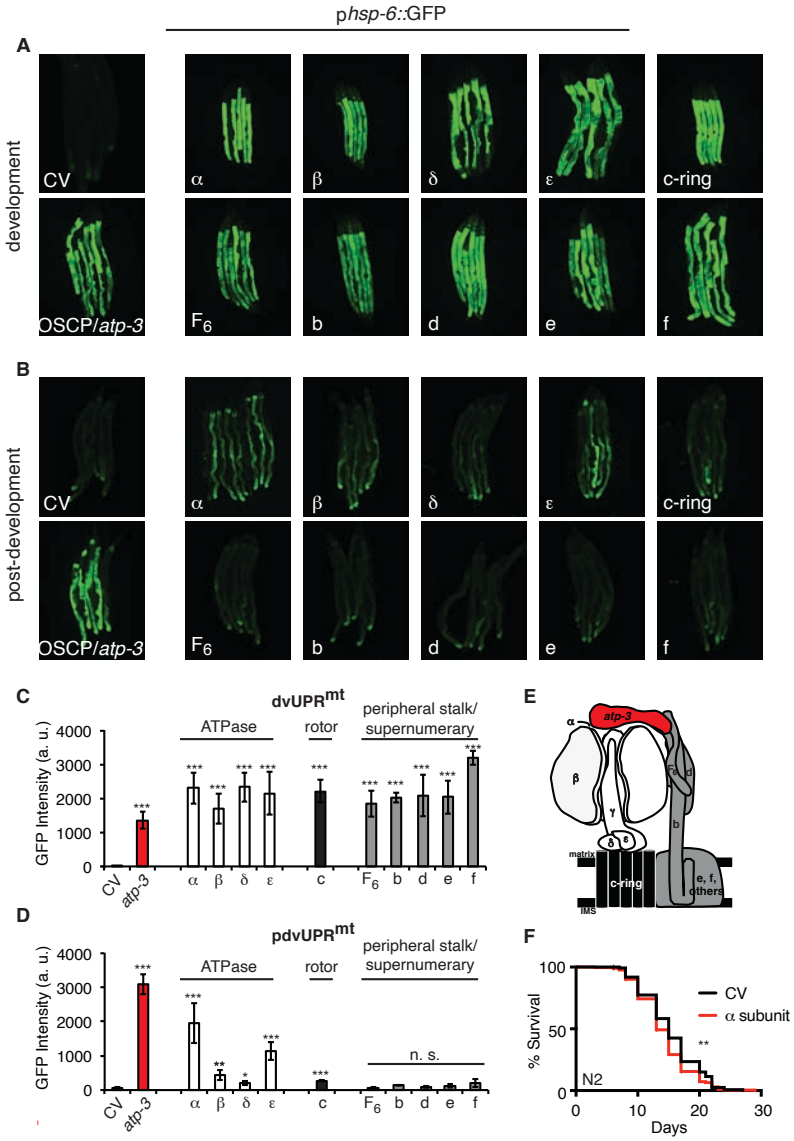

Figure 4: Loss of F-ATP Synthase ATPases Induce a Post-Developmental UPR^{mt}
(A) Developmental RNAi of all ATP synthase subunits tested induced the p*hsp-6*::GFP reporter. For developmental treatment, worms were exposed to RNAi beginning from eggs for 72 hours.
(B) Post-developmental RNAi of ATPase and c-ring subunits but not peripheral stalk or supernumerary subunits of the F-ATP synthase induced the p*hsp-6*::GFP reporter. Worms were exposed to RNAi beginning from young adulthood for 48 hours. post-dev, post-development.
(C) Quantification of GFP intensity from (A). Data are the mean ± SEM of ≤ 15 animals combined from three biological experiments. ***p ≤ .0001 by Student's *t*-test. dv, developmental.
(D) Quantification of GFP intensity from (B). Data are the mean ± SEM of ≤ 15 animals combined from three biological experiments. *p ≤ 0.05, **p ≤ 0.01, and ***p ≤ .0001 by Student's *t*-test. pdv, post-developmental.
(E) Schematic of monomeric F-ATP synthase. White subunits, ATPase; black subunits, H+-rotor/c-ring; grey subunits, peripheral stalk and supernumerary subunits; red subunit, oligomycin sensitivity-conferring protein (OSCP/*atp-3*).
(F) Survival curves of wild-type N2 animals on CV or α/*atp-1* RNAi initiated at young adulthood for 48 hours. Pooled survival curves from four biological experiments. **p ≤ .01 by Log Rank (Mantel Cox). CV, control vector.

observed nearly complete inhibition of the OSCP/*atp-3* RNAi-mediated pdvUPR^{mt} (Figures 5B, D). When we knocked down the ATPase subunits (color coded white) in adults, we observed that loss of the β/*atp-2* subunit robustly suppressed the OSCP/*atp-3* RNAi-mediated pdvUPR^{mt}, possibly due to its role in modulating Ca^{2+} in the mPTP, while loss of α/*atp-1* moderately inhibited the pdvUPR^{mt} (Figure 5B, D). Loss of the ATPase subunits δ/*F58F12.1* or ε/*hpo-18* in adults did not affect the pdvUPR^{mt} (Figure 5B, D). In contrast, dual loss of subunits during development all robustly activated the dvUPR^{mt} (Figures 5A, C). Dual loss of subunits from other OXPHOS complexes (NDUFS3/*nuo-2*, complex I; COX5B/*cco-1*, complex IV) had no effect or slightly increased the dvUPR^{mt} and the pdvUPR^{mt} (Figure 5- figure supplement 5A, B). Thus, we find subunits critical for dimerization (peripheral and supernumerary subunits) and proton translocation (c-ring rotor) are required to transduce the OSCP/*atp-3* RNAi-mediated pdvUPR^{mt}. We also find that the β/*atp-2* subunit, previously found to play an important role in Ca^{2+} mediated mPTP (Giorgio et al., 2017), is required to transduce the OSCP/*atp-3* RNAi-

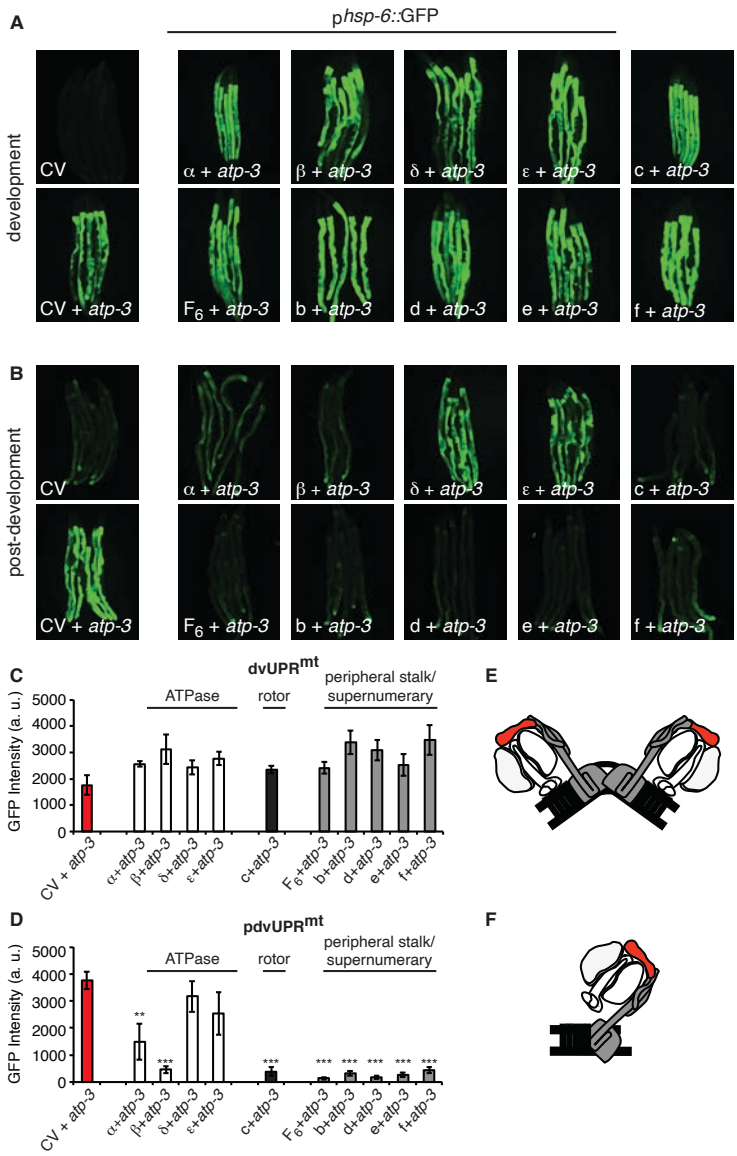

Figure 5: Loss of F-ATP Synthase Subunits Important for the Formation of the mPTP Suppress the Post-Developmental UPR^{mt}
(A, B) Concomitant RNAi of OSCP/*atp-3* and individual F-ATP synthase subunits during developmental (A) or post-developmental (B) inhibited UPR^{mt} to varying degrees in the p*hsp-6*::GFP reporter strain.
(C, D) Quantification of GFP intensity from (A, B). Data are the mean ± SEM of ≤ 15 animals combined from three biological experiments. **p ≤ .001, ***p ≤ 0.0001 compared to CV + *atp-3* condition by Student's *t*-test. dv, developmental, pdv, post-developmental.
(E, F) Models of how F-ATP synthase forms the mPTP as a dimer (E) or monomer (F). White subunits, ATPase; black subunits, H+ rotor/c-ring; grey subunits, peripheral stalk and supernumerary subunits; red subunit, oligomycin sensitivity-conferring protein (OSCP/*atp-3*).

mediated pdvUPR^{mt}. Taken together, these findings support a model in which inhibition of the mPTP via deletion of critical F-ATP synthase subunits inhibits the pdvUPR^{mt}.

To verify that the use of dual-RNAi did not interfere with knockdown of OSCP/*atp-3*, we assessed an endogenously-expressing p*atp-3*::ATP-3::GFP translational reporter generated via CRISPR-Cas-9 (Figure 5- figure supplement 5C). We observed efficient knockdown of ATP-3 via RNAi in the presence of either β/*atp-2* or d/*atp-5* RNAi, two subunits that suppress the pdvUPR^{mt}. These findings demonstrate that inhibition of the pdvUPR^{mt} is not due to ineffective RNAi of OSCP/*atp-3* but rather the functional consequence of removing additional ATP synthase subunits. To examine the effects of dual-RNAi another way, we examined how loss of ATP synthase subunits impacted the pdvUPR^{mt} after α/*atp-1* RNAi, which induced the second most robust pdvUPR^{mt} (Figures 4B, D). Remarkably, we see the same pattern of pdvUPR^{mt} activation and inhibition as with loss of OSCP/*atp-3*: loss of the ATPase subunit β/*atp-2* and peripheral stalk subunit d/*atp-5* suppressed the α/*atp-1* RNAi-mediated pdvUPR^{mt} while loss of

NDUFS3/*nuo-2* and COX5B/*cco-1* had no effect (Figure 5- figure supplement 5D). Importantly, immunoblots against α/*atp-1* showed similar protein knockdown under all conditions (Figure 5- figure supplement 5D), confirming that dual-RNAi is an effective method to assess the structural components of the F-ATP synthase.

Loss of F-ATP Synthase Subunits Important for the Formation of the mPTP Reverse mPTP Characteristics and Regulate Longevity

Based on our observations that loss of peripheral stalk subunits are capable of suppressing the pdvUPR^{mt}, we tested if their loss would also suppress mPTP characteristics. RNAi of peripheral stalk subunits (F6/*atp-4*, d/*atp-5*) or the proton-driving rotor c-ring/*Y82E9BR.3* rescued the loss in MMP, suppressed the rise in cytosolic Ca^{2+}, and rescued the shortened lifespan caused by RNAi of OSCP/*atp-3* (Figures 6A-G and Source Data 1). Interestingly, RNAi of b/*asb-2* did not rescue the loss in membrane potential but did inhibit the rise in cytosolic Ca^{2+} and rescued lifespan (Figures 6A-D and Source Data 1). We further examined the intestinal mitochondrial morphology in worms dually treated with OSCP/*atp-3* and either F6/*atp-4*, d/*atp-5*, or c-ring/*Y82E9BR.3* RNAi. Though RNAi of the peripheral and rotor subunits on its own caused aberrant mitochondrial morphology distinct from controls, RNAi-treatment rescued the rounded and swollen mitochondrial morphology observed due to OSCP/*atp-3* RNAi (Figures 6I-L). Thus, inhibition of key subunits of F-ATP synthase generally reverses the detrimental effects associated with the mPTP/pdvUPR^{mt} nexus.

While testing the epistatic relationship of the F-ATP synthase subunits, we observed that post-developmental RNAi of c-ring/*Y82E9BR.3* on its own was sufficient to significantly extend lifespan (Figure 6H), while the loss of the b/*asb-2*, F6/*atp-4*, and d/*atp-5* peripheral stalk subunits did not (Figure 6- figure supplement 6 and Source Data 1). Similarly, we had previously observed that loss of the α/*atp-1* and β/*atp-2* ATPase subunits had minor lifespan shortening effects (Figures 2H, 3F). Thus, loss of the proton-driving c-ring during adulthood uniquely extends lifespan, which is particularly intriguing due to the fact that a plethora of evidence supports a role for the c-ring as the pore-forming component of mPTP (Alavian et al., 2014; Azarashvili et al., 2014; Bonora et al., 2013; Bonora et al., 2017; Mnatsakanyan et al., 2019; Neginskaya et al., 2019) and its involvement in disease (Amodeo et al., 2021; Licznerski et al., 2020; Morciano et al., 2021).

DISCUSSION

While loss of the F-ATP synthase subunit OSCP/*atp-3* during development leads to lasting activation of the UPR^{mt} and is associated with longevity, we have discovered that loss of this subunit during adulthood induces the mPTP and activates a reversible and *atfs-1*-dependent UPR^{mt} (pdvUPR^{mt}). Furthermore, we observed that activation of the pdvUPR^{mt} helps drive aging. Suppression of the mPTP/UPR^{mt} via genetic or pharmacological interventions is protective. Loss of other OXPHOS subunits or administration of FCCP during adulthood do not cause a loss of the MMP, a rise in cytosolic Ca^{2+}, or activation of the pdvUPR^{mt}, suggesting that the activation of mPTP/UPR^{mt} is specifically due to loss of OSCP/*atp-3*. In contrast, it does not appear that the loss of OSCP/*atp-3* during development activates an mPTP. Thus, loss of OSCP/*atp-3* can have drastically different effects depending on the life stage or cellular milieu of the organism.

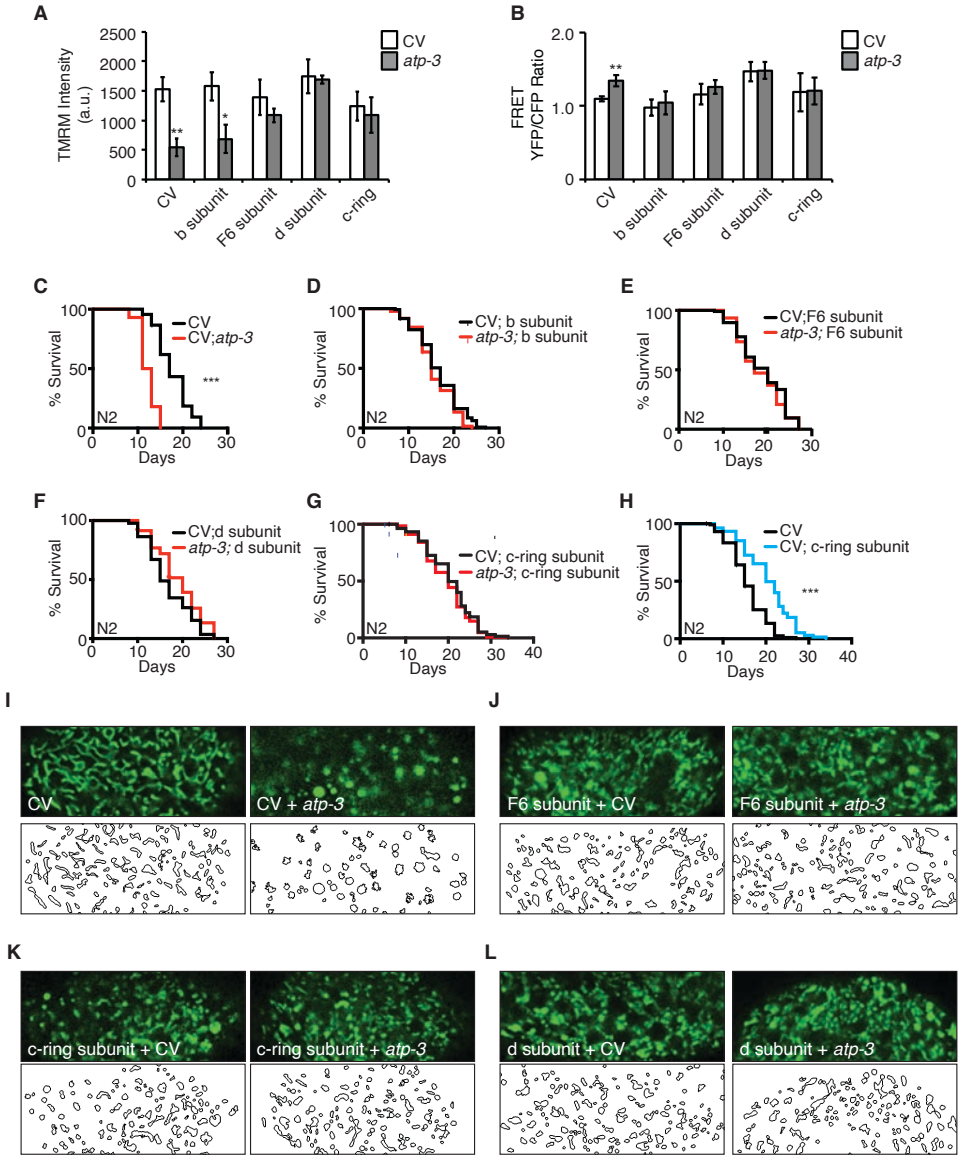

Figure 6: Reversal of mPTP Characteristics and Regulation of Longevity by F-ATP Synthase Subunits
(A) Testing for epistatic interactions between OSCP/*atp-3* and F-ATP synthase subunits on the MMP. RNAis were concomitantly administered beginning at young adulthood for 48 hours. TMRM was spotted on seeded plates. Data are the mean ± SEM of ≤ 15 animals combined from four biological experiments. *p ≤ .05, **p ≤ .01 by Student's *t*-test, CV, control vector.
(B) Testing for epistatic interactions between OSCP/*atp-3* and F-ATP synthase subunits on cytosolic Ca^{2+} using the FRET-based calcium indicator protein D3cpv/cameleon. RNAis were concomitantly administered beginning at young adulthood for 48 hours. Data are the mean ± SEM of ≤ 15 animals combined from three biological experiments. **p ≤ .01 by Student's *t*-test, CV, control vector.
(C-G) Testing for epistatic interactions between OSCP/*atp-3* and F-ATP synthase subunits on the survival. Survival curves of wild-type N2 animals treated with RNAi beginning at young adulthood for 48 hours and then transferred to regular NGM plates for the remainder of the lifespan. Lifespan curves from two pooled biological replicates. ***p ≤ .0001 by Log Rank (Mantel Cox). CV, control vector.
(H) Survival curves of wild-type N2 animals on CV or CV/c-ring subunit. Lifespan curves from two pooled biological replicates. ***p ≤ .0001 by Log Rank (Mantel Cox). CV, control vector RNAi.
(I-L) Testing for epistatic interactions between OSCP/*atp-3* and F-ATP synthase subunits on mitochondrial morphology. Confocal micrographs of intestinal mitochondria labeled with GFP (p*ges-1*::GFP^{mt}) treated with RNAi for 48 hours beginning at young adulthood. Worms were then removed from the RNAi and aged until Day 7 of adulthood followed by collection for microscopy. Top panels, fluorescent channel; bottom panels, rendering of individual mitochondria. See Materials and Methods for details on rendering.

While the mPTP's detrimental effects on health is well established, considerable evidence suggests that the UPR^{mt} contributes to health and longevity (Houtkooper et al., 2013; Merkwirth et al., 2016; Mouchiroud et al., 2013; Sorrentino et al., 2017). Activating the UPR^{mt} in neurons can activate protective cell non-autonomous signals and also epigenetically rewire *C. elegans* to live longer (Durieux et al., 2011; Merkwirth et al., 2016; Tian et al., 2016; Zhang et al., 2018). NAD^+ boosters activate a UPR^{mt} that contributes to longevity and ameliorates AD (Mouchiroud et al., 2013; Sorrentino et al., 2017). However, an unbiased screen that identified activators of the UPR^{mt} found no correlation between UPR^{mt} activation and longevity (Bennett et al., 2014) and constitutive activation of the UPR^{mt} in dopaminergic neurons led to increased neurodegeneration (Martinez et al., 2017). Activation of the UPR^{mt} in our setting is distinct in that it is specifically linked to activation of the mPTP. Thus, it is possible that preemptively boosting the UPR^{mt} may ward off aging and disease while activation during a diseased setting may exacerbate conditions, akin to instances of inflammation in disease.

We propose a model in which loss of OSCP/*atp-3* induces a conformational change in F-ATP synthase that leads to pore formation and activation of the UPR^{mt} during adulthood but not during development. Previous reports have shown that loss of OSCP increases susceptibility to Ca^{2+}-induced mPTP formation and that key residues within the OSCP are required to suppress the mPTP during conditions of low pH (Antoniel et al., 2018; Giorgio et al., 2013), suggesting that a functional and intact OSCP protects against pore formation. OSCP levels have also been shown to decrease with age while concomitantly increasing its binding to amyloid β, suggesting that loss of OSCP destabilizes the remaining F-ATP synthase to increase pore formation (Beck et al., 2016b). However, it has also been shown that OSCP provides the binding site for cyclophilin D and thus it has been proposed to be critical in the formation of the mPTP (Giorgio et al., 2009; Giorgio et al., 2013). However, immunoprecipitation studies show that cyclophilin D my also bind the peripheral stalk subunit b, which is also supported by EM studies (Daum et al., 2013; Giorgio et al., 2013). Thus, our findings support a model in which loss of OSCP/*atp-3* induces a conformation change that is favorable for cyclophilin binding to the remaining peripheral stalk proteins or to sites independent of the F-ATP synthase, leading to destabilization of ATP synthase, pore formation with a loss of MMP, and subsequent activation of the $pdvUPR^{mt}$.

The loss of OSCP/*atp-3* may also be more impactful than other subunits. Unlike other F-ATP synthase subunits, OSCP/*atp-3* is prominently accessible in the mitochondrial matrix and has a diverse set of binding partners, such as estradiol and p53, which can modulate ATP production (Bergeaud et al., 2013; Zheng and Ramirez, 1999). Its loss may induce a strong protein misfolding cascade, reminiscent of the He and Lemasters mPTP model first proposed in 2002 (He and Lemasters, 2002). In this model, it was proposed that exposure to activators of the mPTP, such as oxidants, causes protein misfolding of integral membrane proteins, thereby recruiting chaperones such as cyclophilin D to repair. If the protein misfolding is unable to be repaired, then Ca^{2+}, along with cyclophilin D, could catalyze pore formation in a CsA-dependent manner. Indeed, both paraquat and manganese have been shown to induce both the UPR^{mt} and the mPTP in separate studies (Angeli et al., 2014; Costantini et al., 1995; Nargund et al., 2012; Rao and Norenberg, 2004). However, more research is needed to clarify the relationship between protein misfolding and the mPTP.

AD and PD both display evidence of the mPTP and in some instances, elevated UPR^{mt} profiles have also been observed (Beck et al., 2016a; Beck et al., 2016b; Ludtmann et al., 2018; Perez et al., 2018; Sorrentino et al., 2017), but the relationship between these two mitochondrial processes have not been fully explored. Ischemic reperfusion injuries directly cause the mPTP but little is known about the UPR^{mt} under these conditions (Kaufman and Crowder, 2015). Establishing a clearer understanding of the relationship between the UPR^{mt} and the mPTP in these disease states could result in the development of new therapeutics for these and related disorders.

ACKNOWLEDGEMENTS

We thank members of the Lithgow and Andersen labs for helpful discussion and advice on this research and the Buck Institute morphology department for their core services. *C. elegans* strains used in this work were provided by the *Caenorhabditis* Genetics Center (CGC), funded by the NIH Office of Research Infrastructure Programs (P40OD010440), and the Japanese National BioResource Project. The Y82E9BR.3 RNAi clone was a generous gift from Dr. Seung-Jae V. Lee from the Seoul National University College of Medicine. This work was supported by NIH grants RFAG057358 and R01AG029631 and the Larry L. Hillblom Foundation.

AUTHOR CONTRIBUTIONS

Conceptualization, S.A., J.K.A., and G.J.L.; Methodology, S.A., J.K.A., G.J.L., and A.C.F.; Investigation, S.A., A.C.F., T.H.P., M.C., D.B. and A.A.S., Validation, S.A. and A.C.F.; Resources, A.A.G.; Writing –Original Draft, S.A., J.K.A., and G.J.L.; Writing – Revised Draft, S.A., J.K.A., and G.J.L; Visualization, S.A., Supervision, S.A., J.K.A, G.L., Funding Acquisition, J.K.A. and G.J.L.

DECLARATION OF INTEREST

G.J.L. is cofounder of GeroState alpha and declares no financial interest related to this work. A.A.G. is founder of Image Analyst MKII Software and declares a financial interest.

MATERIAL AND METHODS

KEY RESOURCES

Chemicals		
Tetramethylrhodamine methyl ester (perchlorate) (TMRM)	Cayman Chemical	Item # 21437
Cyclosporin A	Cayman Chemical	Item # 12088
FK506 (Tacrolimus)	Cayman Chemical	Item # 10007965
FCCP (Trifluoromethoxy carbonylcyanide phenylhydrazone)	Cayman Chemical	Item # 15218
Antibodies		
Mouse monoclonal anti-GRP 75 (D9)	Santa Cruz Biotechnology	Cat# sc-133137
Mouse monoclonal anti-β Tubulin Antibody (D-10)	Santa Cruz Biotechnology	Cat# sc-5274
Mouse monoclonal anti-β-Actin (8H10D10)	Cell Signaling Technology	Cat# 3700
Mouse monoclonal anti- ATP5A1 Monoclonal Antibody (15H4C4)	Invitrogen	Cat# 43-9800

Mouse monoclonal anti-ATP Synthase beta Monoclonal Antibody (3D5AB1)	Invitrogen	Cat# A-21351
Mouse monoclonal anti-NDUFS3 Monoclonal Antibody (17D95)	Invitrogen	Cat# 43-9200
Experimental Models: Organisms/Strains		
C. *elegans*: N2 Bristol	Caenorhabditis Genetics Center	RRID:WB-STRAIN:N2_(anscestral)
C. *elegans*: SJ4100 (zcIs13[*hsp-6*p::GFP])	Caenorhabditis Genetics Center	RRID:WB-STRAIN:SJ4100
C. *elegans*: SJ4058 (zcIs9[*hsp-60*p::GFP + *lin-15(+)*])	Caenorhabditis Genetics Center	RRID:WB-STRAIN:SJ4058
C. *elegans*: SJ4005 (zcIs4[*hsp-4*p::GFP])	Caenorhabditis Genetics Center	RRID:WB-STRAIN:VC1099
C. *elegans*: CL2070 (dvIs[*hsp-16.2*p::GFP])	Caenorhabditis Genetics Center	RRID:WB-STRAIN:CL2070
C. *elegans*: KWN190 (rnyEx109[*nhx-2*p::D3cpv + *pha-1*(+)], *pha-1(e2123) III; him-5(e1490)* V)	Caenorhabditis Genetics Center	RRID:WB-STRAIN:KWN190
C. *elegans*: ZC376.7 *atfs-1(tm4525)*	National BioResource Project	N/A
C. *elegans*: PHX1826 (qIs48[*atp-3(syb1826)*/hT2[*bli-4(e937) let-?(q782)*])	SunyBiotech	N/A
C. elegans: SJ4143 (zcls17 [*ges-1*p::GFP(mt)])	Caenorhabditis Genetics Center	RRID:WB-STRAIN:SJ4143
C. elegans: GL347 (SJ4100 (zcIs13[*hsp-6*p::GFP]) BC 6x to N2 Bristol)	This Study	N/A

CONTACT FOR REAGENT AND RESOURCE SHARING

Further information and requests for resources and reagents should be directed to and will be fulfilled by the Lead Contacts, Gordon Lithgow, glithgow@buckinstitute.org, Julie Andersen, jandersen@buckinstitute.org, and Suzanne Angeli, sangeli@buckinstitute.org

EXPERIMENTAL MODEL AND SUBJECT DETAILS

Nematode Strains

The following strain was obtained from the National BioResource Project: *atfs-1(tm4525)*. The following strains were obtained from the *Caenorhabditis* Genetic Center (CGC): SJ4100 (zcIs13[*hsp-6*p::GFP]), SJ4058 (zcIs9[*hsp-60*p::GFP]), SJ4005 (zcIs4[*hsp-4*p::GFP]), CL2070 (dvIs[*hsp-16.2*p::GFP]), SJ4143 (zcls17 [*ges-1*p::GFP(mt)]), KWN190 ([*pha-1*(*e2123*) III]; [*him-5*(*e1490*) V]; rnyEx109), CL2070 (dvIs70[*hsp-16.2p*::GFP], [*rol-6*(su1006)]), SJ4005 (zcls4[*hsp-4*::GFP]), and N2 Bristol (wild-type). The following strain, SJ4100 (zcIs13[*hsp-6*p::GFP]) was backcrossed 6 times to wild-type N2 to generate GL347, which was used for all *hsp-6*p::GFP experiments.

CRISPR-Cas9 strain

The translational *atp-3*p::ATP-3::GFP was generated by SunyBiotech (http://www.sunybiotech.com/) using CRISPR-Cas9. The strain PHX1826 *atp-3(syb1826)*/hT2[*bli-4(e937) let-?(q782)* qIs48] was verified by PCR sequencing. The sgRNA target site used is as follows:
Sg1: CCCTTGCCACCGCCATCTAAatt

Sg2:CCGCCATCTAAatttttcccaaa.

Nematode and Bacterial Culture Conditions
Nematodes were maintained on nematode growth medium (NGM) plates. NGM plates were seeded with *E. coli* OP50 obtained from CGC that was grown in LB broth at 37˚C for 18 hours shaking at 225 rpm. Plates with bacteria were dried for 48 hours before use.

For RNAi experiments, *E. coli* HT115 (DE3) bacteria obtained from the Ahringer and Vidal RNAi Library was used (Kamath et al., 2003; Rual et al., 2004). All RNAi clones were verified via sequencing (Eurofins™). RNAi plates were prepared by cooling NGM to 55˚C and supplementing with a final concentration of 50ug/ml carbenicillin and 1mM Isopropyl β- d-1-thiogalactopyranoside (IPTG). RNAi bacteria was inoculated with one colony of RNAi bacteria into LB with 50ug/ml carbenicillin and was grown shaking overnight for 18 hours at 37˚ at 225 rpm.

Post-Developmental Timing
To achieve synchronous nematode populations, day 1 adult nematodes were allowed to lay eggs for 2 hours on seeded NGM plates. For convenience, nematodes were developed at 25˚C on *E. coli* OP50 until worms were visibly past the L4 stage (loss of crescent) but not yet gravid, approximately 45 hours for wild-type (although the time it takes for the worms to reach the young adult stage varies by strain). Nematodes were shifted to 20˚C once they reached adulthood.

METHOD DETAILS

RNA Interference (RNAi) Treatment
For developmental treatments, synchronized eggs were moved onto plates seeded with RNAi bacteria and developed at 20˚C for 72 hours. Nematodes were then either collected for analysis or for lifespans, remained on RNAi bacteria for the remainder of their life for survival analysis. For post-developmental treatments, synchronized eggs were developed on plates with *E. coli* OP50 at 25˚C until the young adult stage and then transferred to RNAi plates at 20˚C. Nematodes were collected after 48 hours for analysis or for lifespans, moved onto *E. coli* OP50 for the remainder of their life.

Quantitative RT-PCR
Approximately 300 adult nematodes were collected; nematode pellets were resuspended in 300uL RNA Lysis Buffer and frozen. Pellets was thawed, vortexed, and snap frozen three times. Zymo Research Quick-RNA MiniPrep kit was used to extract RNA. The primers used for qPCR are as follows:
act-1, Forward: ACGACGAGTCCGGCCCATCC
act-1, Reverse: GAAAGCTGGTGGTGACGATGGTT
atp-1, Forward: GAAGGACAAATCTCCCCACA
atp-2, Reverse: CGCCACATTCTTCCTTTTTC
atp-3, Forward: GCCTAATTTCTTAATTTTGCAGGT
atp-3, Reverse: GAACCTGAATCGGGGTCTTC
atp-4, Forward: AATATGTTGCCTCCCGTGAT

atp-4, Reverse: GGAACAAAAACGTTCATTCG
atp-5, Forward: TCTTCGACGTGCCGACAA
atp-5, Reverse: AAATGGTAGGAGAGCGATAAGG
nuo-2, Forward: TGAAGTTGCTGAGCCAACAC
nuo-2, Reverse: TCCACACTAACAGAAAATGAGTCT
cco-1, Forward: TTTCGGCTATTGTTCGCATT
cco-1, Reverse: GCCGTCTTAGCAAGTTGAGC

Lifespans
Day 1 adult nematodes were allowed to lay eggs for 2 hours on seeded NGM plates to obtain a synchronous aging population. 5-fluoro-2-deoxyuridine (FUdR) was omitted from plates due to its potentially confounding effects (Angeli et al., 2013). Worms are transferred to freshly seeded bacterial plates every day for the first 7 days of adulthood and then as needed afterwards. Worms were scored as dead when they failed to respond to gentle prodding with a platinum wire. Worms that experienced matricide or bagging were censored.

Tetramethylrhodamine Methyl Ester (TMRM) Staining
Plates were prepared by spotting seeded NGM plates with a TMRM solution diluted in water to a final concentration of 0.1 μM in the plates. Water was used as a solvent control. Plates were allowed to dry for 24 hours before use. For developmental experiments, synchronized eggs were placed on plates for 72 hours and then nematodes were collected for analysis. For post-developmental experiments, young adult nematodes were placed on plates for 48 hours and then collected for analysis.

Cyclosporin A (CsA) Treatment
Plates were prepared by spotting seeded NGM plates with a CsA (stock solution in DMSO) solution diluted in 100% ethanol. Comparable amounts of DMSO and ethanol were used as solvent controls. Plates were allowed to dry for 24 hours before use. For developmental experiments, synchronized eggs were placed on plates for 72 hours and then nematodes were collected for analysis. For post-developmental experiments, young adult nematodes were placed on plates for 48 hours and then collected for analysis; for lifespans, worms were moved to regular NGM plates for the remainder of their life after 48 hours on drug-treated RNAi bacteria.

Microscopy
Worms were anesthetized with 2mM levamisole and mounted on 2% agarose pads on glass slides. Fluorescence micrographs of GFP and TMRM were taken using a Zeiss Imager A2 at 5x magnification with 600ms exposure using the ZEN software. GFP expression was enhanced using the brightness/contrast tool in Photoshop. The same parameters were used for all images.

Confocal micrographs of mitochondrially targeted GFP and the cytosolic calcium sensor D3cpv (Zhang et al., 2016) were taken using a Zeiss LSM780 laser scanning confocal microscope using a 63× Plan Apochromat NA1.4. To visualize outlines of mitochondria, Image Analyst MKII (Image Analyst Software, Novato, CA) was used. Selected rectangular regions of interest (ROI) from the worm intestine were segmented and converted to outlines by a modification of the "Segment mitochondria" pipeline. Emission ratio images of D3cpv were excited at 440nm and

captured at 450-490nm and 520-560nm and analyzed in Image Analyst MKII. Images were Wiener filtered and the ratio of the 540nm over the 470nm channel, indicative of cytosolic calcium concertation was calculated, and showed in pseudo-color coding. Emission ratios were determined in ROIs in the posterior intestine by the Plot Ratio function.

Western Blot

Approximately 30 to 50 adult worms were collected in S-basal buffer. Supernatant was removed and nematodes were flash-frozen. Worms pellets were resuspended in 2% SDS sample buffer with 2.5% β–mercaptoethanol and samples were boiled for 10 minutes. Samples were subjected to SDS-PAGE using 4-12% SDS gels (Invitrogen™) and transferred to Immun-Blot PVDF Membrane (BIO-RAD™) using BIO-RAD™ western blot Criterion apparatus. Membranes were blocked with 5% non-fat dry milk blocking solution; concentrations for antibodies were 1:1000 for primary antibodies and 1:2000 for secondary antibodies.

QUANTIFICATION, STATISTICS, AND PREDICTION

Statistics

Significance between control and experimental groups was determined by using two-tailed Student's t test. Asterisks denote corresponding statistical significance *$p < 0.05$; **$p < 0.01$; ***$p < 0.0001$. Error bars were generated using the standard error of the mean (SEM), typically from three pooled biological replicates. Graphpad Prism 7™ was used to plot survival curves. Log Rank (Mantel Cox) test in Prism™ was used to determine significance between the control and experimental group.

GFP Quantification

GFP intensity of worms was quantified using Image J 1.52A. The 'integrated density' of GFP expression and length of worms was measured using Image J tools. Integrated Density value was normalized by number of worms and average length of worms. The final value is in arbitrary units.

Mitochondrial Targeting Prediction

Mitochondrial presequences were predicted using the MitoFates tool (Fukasawa et al., 2015).

REFERENCES

Alavian, K.N., Beutner, G., Lazrove, E., Sacchetti, S., Park, H.A., Licznerski, P., Li, H., Nabili, P., Hockensmith, K., Graham, M., *et al.* (2014). An uncoupling channel within the c-subunit ring of the F1FO ATP synthase is the mitochondrial permeability transition pore. Proceedings of the National Academy of Sciences of the United States of America *111*, 10580-10585.
Amodeo, G.F., Lee, B.Y., Krilyuk, N., Filice, C.T., Valyuk, D., Otzen, D.E., Noskov, S., Leonenko, Z., and Pavlov, E.V. (2021). C subunit of the ATP synthase is an amyloidogenic calcium dependent channel-forming peptide with possible implications in mitochondrial permeability transition. Sci Rep *11*, 8744.
Angeli, S., Barhydt, T., Jacobs, R., Killilea, D.W., Lithgow, G.J., and Andersen, J.K. (2014). Manganese disturbs metal and protein homeostasis in Caenorhabditis elegans. Metallomics *6*, 1816-1823.

Angeli, S., Klang, I., Sivapatham, R., Mark, K., Zucker, D., Bhaumik, D., Lithgow, G.J., and Andersen, J.K. (2013). A DNA synthesis inhibitor is protective against proteotoxic stressors via modulation of fertility pathways in Caenorhabditis elegans. Aging (Albany NY) *5*, 759-769.
Antoniel, M., Jones, K., Antonucci, S., Spolaore, B., Fogolari, F., Petronilli, V., Giorgio, V., Carraro, M., Di Lisa, F., Forte, M.*, et al.* (2018). The unique histidine in OSCP subunit of F-ATP synthase mediates inhibition of the permeability transition pore by acidic pH. EMBO Rep *19*, 257-268.
Azarashvili, T., Odinokova, I., Bakunts, A., Ternovsky, V., Krestinina, O., Tyynela, J., and Saris, N.E. (2014). Potential role of subunit c of F0F1-ATPase and subunit c of storage body in the mitochondrial permeability transition. Effect of the phosphorylation status of subunit c on pore opening. Cell Calcium *55*, 69-77.
Baines, C.P., Kaiser, R.A., Purcell, N.H., Blair, N.S., Osinska, H., Hambleton, M.A., Brunskill, E.W., Sayen, M.R., Gottlieb, R.A., Dorn, G.W.*, et al.* (2005). Loss of cyclophilin D reveals a critical role for mitochondrial permeability transition in cell death. Nature *434*, 658-662.
Baker, B.M., Nargund, A.M., Sun, T., and Haynes, C.M. (2012). Protective coupling of mitochondrial function and protein synthesis via the eIF2alpha kinase GCN-2. PLoS genetics *8*, e1002760.
Basso, E., Fante, L., Fowlkes, J., Petronilli, V., Forte, M.A., and Bernardi, P. (2005). Properties of the permeability transition pore in mitochondria devoid of Cyclophilin D. The Journal of biological chemistry *280*, 18558-18561.
Beck, J.S., Mufson, E.J., and Counts, S.E. (2016a). Evidence for Mitochondrial UPR Gene Activation in Familial and Sporadic Alzheimer's Disease. Curr Alzheimer Res *13*, 610-614.
Beck, S.J., Guo, L., Phensy, A., Tian, J., Wang, L., Tandon, N., Gauba, E., Lu, L., Pascual, J.M., Kroener, S.*, et al.* (2016b). Deregulation of mitochondrial F1FO-ATP synthase via OSCP in Alzheimer's disease. Nat Commun *7*, 11483.
Bennett, C.F., Vander Wende, H., Simko, M., Klum, S., Barfield, S., Choi, H., Pineda, V.V., and Kaeberlein, M. (2014). Activation of the mitochondrial unfolded protein response does not predict longevity in Caenorhabditis elegans. Nat Commun *5*, 3483.
Bergeaud, M., Mathieu, L., Guillaume, A., Moll, U.M., Mignotte, B., Le Floch, N., Vayssiere, J.L., and Rincheval, V. (2013). Mitochondrial p53 mediates a transcription-independent regulation of cell respiration and interacts with the mitochondrial F(1)F0-ATP synthase. Cell Cycle *12*, 2781-2793.
Bernardi, P., and Di Lisa, F. (2015). The mitochondrial permeability transition pore: molecular nature and role as a target in cardioprotection. J Mol Cell Cardiol *78*, 100-106.
Bonora, M., Bononi, A., De Marchi, E., Giorgi, C., Lebiedzinska, M., Marchi, S., Patergnani, S., Rimessi, A., Suski, J.M., Wojtala, A.*, et al.* (2013). Role of the c subunit of the FO ATP synthase in mitochondrial permeability transition. Cell Cycle *12*, 674-683.
Bonora, M., Morganti, C., Morciano, G., Pedriali, G., Lebiedzinska-Arciszewska, M., Aquila, G., Giorgi, C., Rizzo, P., Campo, G., Ferrari, R.*, et al.* (2017). Mitochondrial permeability transition involves dissociation of F1FO ATP synthase dimers and C-ring conformation. EMBO Rep *18*, 1077-1089.
Carraro, M., Checchetto, V., Szabo, I., and Bernardi, P. (2019). F-ATP synthase and the permeability transition pore: fewer doubts, more certainties. FEBS Lett *593*, 1542-1553.
Carraro, M., Giorgio, V., Sileikyte, J., Sartori, G., Forte, M., Lippe, G., Zoratti, M., Szabo, I., and Bernardi, P. (2014). Channel formation by yeast F-ATP synthase and the role of

dimerization in the mitochondrial permeability transition. The Journal of biological chemistry *289*, 15980-15985.
Carroll, J., He, J., Ding, S., Fearnley, I.M., and Walker, J.E. (2019). Persistence of the permeability transition pore in human mitochondria devoid of an assembled ATP synthase. Proceedings of the National Academy of Sciences of the United States of America *116*, 12816-12821.
Costantini, P., Petronilli, V., Colonna, R., and Bernardi, P. (1995). On the effects of paraquat on isolated mitochondria. Evidence that paraquat causes opening of the cyclosporin A-sensitive permeability transition pore synergistically with nitric oxide. Toxicology *99*, 77-88.
Daum, B., Walter, A., Horst, A., Osiewacz, H.D., and Kuhlbrandt, W. (2013). Age-dependent dissociation of ATP synthase dimers and loss of inner-membrane cristae in mitochondria. Proceedings of the National Academy of Sciences of the United States of America *110*, 15301-15306.
Dillin, A., Hsu, A.L., Arantes-Oliveira, N., Lehrer-Graiwer, J., Hsin, H., Fraser, A.G., Kamath, R.S., Ahringer, J., and Kenyon, C. (2002). Rates of behavior and aging specified by mitochondrial function during development. Science (New York, NY *298*, 2398-2401.
Durieux, J., Wolff, S., and Dillin, A. (2011). The cell-non-autonomous nature of electron transport chain-mediated longevity. Cell *144*, 79-91.
Farina, F., Alberti, A., Breuil, N., Bolotin-Fukuhara, M., Pinto, M., and Culetto, E. (2008). Differential expression pattern of the four mitochondrial adenine nucleotide transporter ant genes and their roles during the development of Caenorhabditis elegans. Dev Dyn *237*, 1668-1681.
Fukasawa, Y., Tsuji, J., Fu, S.C., Tomii, K., Horton, P., and Imai, K. (2015). MitoFates: improved prediction of mitochondrial targeting sequences and their cleavage sites. Mol Cell Proteomics *14*, 1113-1126.
Gauba, E., Guo, L., and Du, H. (2017). Cyclophilin D Promotes Brain Mitochondrial F1FO ATP Synthase Dysfunction in Aging Mice. J Alzheimers Dis *55*, 1351-1362.
Giorgio, V., Bisetto, E., Soriano, M.E., Dabbeni-Sala, F., Basso, E., Petronilli, V., Forte, M.A., Bernardi, P., and Lippe, G. (2009). Cyclophilin D modulates mitochondrial F0F1-ATP synthase by interacting with the lateral stalk of the complex. The Journal of biological chemistry *284*, 33982-33988.
Giorgio, V., Burchell, V., Schiavone, M., Bassot, C., Minervini, G., Petronilli, V., Argenton, F., Forte, M., Tosatto, S., Lippe, G.*, et al.* (2017). Ca(2+) binding to F-ATP synthase beta subunit triggers the mitochondrial permeability transition. EMBO Rep *18*, 1065-1076.
Giorgio, V., von Stockum, S., Antoniel, M., Fabbro, A., Fogolari, F., Forte, M., Glick, G.D., Petronilli, V., Zoratti, M., Szabo, I.*, et al.* (2013). Dimers of mitochondrial ATP synthase form the permeability transition pore. Proceedings of the National Academy of Sciences of the United States of America *110*, 5887-5892.
Guo, L., Carraro, M., Carrer, A., Minervini, G., Urbani, A., Masgras, I., Tosatto, S.C.E., Szabo, I., Bernardi, P., and Lippe, G. (2019). Arg-8 of yeast subunit e contributes to the stability of F-ATP synthase dimers and to the generation of the full-conductance mitochondrial megachannel. The Journal of biological chemistry *294*, 10987-10997.
Guo, Y., Zhang, K., Gao, X., Zhou, Z., Liu, Z., Yang, K., Huang, K., Yang, Q., and Long, Q. (2020). Sustained oligomycin sensitivity conferring protein expression in cardiomyocytes protects

against cardiac hypertrophy induced by pressure-overload via improving mitochondrial function. Hum Gene Ther.
Haynes, C.M., Yang, Y., Blais, S.P., Neubert, T.A., and Ron, D. (2010). The matrix peptide exporter HAF-1 signals a mitochondrial UPR by activating the transcription factor ZC376.7 in C. elegans. Molecular cell *37*, 529-540.
He, J., Carroll, J., Ding, S., Fearnley, I.M., and Walker, J.E. (2017a). Permeability transition in human mitochondria persists in the absence of peripheral stalk subunits of ATP synthase. Proceedings of the National Academy of Sciences of the United States of America *114*, 9086-9091.
He, J., Ford, H.C., Carroll, J., Ding, S., Fearnley, I.M., and Walker, J.E. (2017b). Persistence of the mitochondrial permeability transition in the absence of subunit c of human ATP synthase. Proceedings of the National Academy of Sciences of the United States of America *114*, 3409-3414.
He, L., and Lemasters, J.J. (2002). Regulated and unregulated mitochondrial permeability transition pores: a new paradigm of pore structure and function? FEBS Lett *512*, 1-7.
Houtkooper, R.H., Mouchiroud, L., Ryu, D., Moullan, N., Katsyuba, E., Knott, G., Williams, R.W., and Auwerx, J. (2013). Mitonuclear protein imbalance as a conserved longevity mechanism. Nature *497*, 451-457.
Iurlaro, R., and Munoz-Pinedo, C. (2016). Cell death induced by endoplasmic reticulum stress. FEBS J *283*, 2640-2652.
Kamath, R.S., Fraser, A.G., Dong, Y., Poulin, G., Durbin, R., Gotta, M., Kanapin, A., Le Bot, N., Moreno, S., Sohrmann, M.*, et al.* (2003). Systematic functional analysis of the Caenorhabditis elegans genome using RNAi. Nature *421*, 231-237.
Karch, J., Bround, M.J., Khalil, H., Sargent, M.A., Latchman, N., Terada, N., Peixoto, P.M., and Molkentin, J.D. (2019). Inhibition of mitochondrial permeability transition by deletion of the ANT family and CypD. Sci Adv *5*, eaaw4597.
Kaufman, D.M., and Crowder, C.M. (2015). Mitochondrial Proteostatic Collapse Leads to Hypoxic Injury. Curr Biol *25*, 2171-2176.
Kim, H.E., Grant, A.R., Simic, M.S., Kohnz, R.A., Nomura, D.K., Durieux, J., Riera, C.E., Sanchez, M., Kapernick, E., Wolff, S.*, et al.* (2016). Lipid Biosynthesis Coordinates a Mitochondrial-to-Cytosolic Stress Response. Cell *166*, 1539-1552 e1516.
Kwong, J.Q., and Molkentin, J.D. (2015). Physiological and pathological roles of the mitochondrial permeability transition pore in the heart. Cell Metab *21*, 206-214.
Labbadia, J., and Morimoto, R.I. (2015). Repression of the Heat Shock Response Is a Programmed Event at the Onset of Reproduction. Molecular cell *59*, 639-650.
Licznerski, P., Park, H.A., Rolyan, H., Chen, R., Mnatsakanyan, N., Miranda, P., Graham, M., Wu, J., Cruz-Reyes, N., Mehta, N.*, et al.* (2020). ATP Synthase c-Subunit Leak Causes Aberrant Cellular Metabolism in Fragile X Syndrome. Cell *182*, 1170-1185 e1179.
Lin, Y.F., Schulz, A.M., Pellegrino, M.W., Lu, Y., Shaham, S., and Haynes, C.M. (2016). Maintenance and propagation of a deleterious mitochondrial genome by the mitochondrial unfolded protein response. Nature *533*, 416-419.
Liu, J., Farmer, J.D., Jr., Lane, W.S., Friedman, J., Weissman, I., and Schreiber, S.L. (1991). Calcineurin is a common target of cyclophilin-cyclosporin A and FKBP-FK506 complexes. Cell *66*, 807-815.
Ludtmann, M.H.R., Angelova, P.R., Horrocks, M.H., Choi, M.L., Rodrigues, M., Baev, A.Y., Berezhnov, A.V., Yao, Z., Little, D., Banushi, B.*, et al.* (2018). alpha-synuclein oligomers

interact with ATP synthase and open the permeability transition pore in Parkinson's disease. Nat Commun *9*, 2293.
Martinez, B.A., Petersen, D.A., Gaeta, A.L., Stanley, S.P., Caldwell, G.A., and Caldwell, K.A. (2017). Dysregulation of the Mitochondrial Unfolded Protein Response Induces Non-Apoptotic Dopaminergic Neurodegeneration in C. elegans Models of Parkinson's Disease. J Neurosci *37*, 11085-11100.
Merkwirth, C., Jovaisaite, V., Durieux, J., Matilainen, O., Jordan, S.D., Quiros, P.M., Steffen, K.K., Williams, E.G., Mouchiroud, L., Tronnes, S.U.*, et al.* (2016). Two Conserved Histone Demethylases Regulate Mitochondrial Stress-Induced Longevity. Cell *165*, 1209-1223.
Mnatsakanyan, N., and Jonas, E.A. (2020). ATP synthase c-subunit ring as the channel of mitochondrial permeability transition: Regulator of metabolism in development and degeneration. J Mol Cell Cardiol *144*, 109-118.
Mnatsakanyan, N., Llaguno, M.C., Yang, Y., Yan, Y., Weber, J., Sigworth, F.J., and Jonas, E.A. (2019). A mitochondrial megachannel resides in monomeric F1FO ATP synthase. Nat Commun *10*, 5823.
Morciano, G., Pedriali, G., Bonora, M., Pavasini, R., Mikus, E., Calvi, S., Bovolenta, M., Lebiedzinska-Arciszewska, M., Pinotti, M., Albertini, A.*, et al.* (2021). A naturally occurring mutation in ATP synthase subunit c is associated with increased damage following hypoxia/reoxygenation in STEMI patients. Cell Rep *35*, 108983.
Mouchiroud, L., Houtkooper, R.H., Moullan, N., Katsyuba, E., Ryu, D., Canto, C., Mottis, A., Jo, Y.S., Viswanathan, M., Schoonjans, K.*, et al.* (2013). The NAD(+)/Sirtuin Pathway Modulates Longevity through Activation of Mitochondrial UPR and FOXO Signaling. Cell *154*, 430-441.
Munch, C., and Harper, J.W. (2016). Mitochondrial unfolded protein response controls matrix pre-RNA processing and translation. Nature *534*, 710-713.
Murphy, B.J., Klusch, N., Langer, J., Mills, D.J., Yildiz, O., and Kuhlbrandt, W. (2019). Rotary substates of mitochondrial ATP synthase reveal the basis of flexible F1-Fo coupling. Science (New York, NY *364*.
Nakagawa, T., Shimizu, S., Watanabe, T., Yamaguchi, O., Otsu, K., Yamagata, H., Inohara, H., Kubo, T., and Tsujimoto, Y. (2005). Cyclophilin D-dependent mitochondrial permeability transition regulates some necrotic but not apoptotic cell death. Nature *434*, 652-658.
Naresh, N.U., and Haynes, C.M. (2019). Signaling and Regulation of the Mitochondrial Unfolded Protein Response. Cold Spring Harb Perspect Biol *11*.
Nargund, A.M., Pellegrino, M.W., Fiorese, C.J., Baker, B.M., and Haynes, C.M. (2012). Mitochondrial import efficiency of ATFS-1 regulates mitochondrial UPR activation. Science (New York, NY *337*, 587-590.
Neginskaya, M.A., Solesio, M.E., Berezhnaya, E.V., Amodeo, G.F., Mnatsakanyan, N., Jonas, E.A., and Pavlov, E.V. (2019). ATP Synthase C-Subunit-Deficient Mitochondria Have a Small Cyclosporine A-Sensitive Channel, but Lack the Permeability Transition Pore. Cell Rep *26*, 11-17 e12.
Nicolli, A., Basso, E., Petronilli, V., Wenger, R.M., and Bernardi, P. (1996). Interactions of cyclophilin with the mitochondrial inner membrane and regulation of the permeability transition pore, and cyclosporin A-sensitive channel. The Journal of biological chemistry *271*, 2185-2192.
Ong, S.B., Samangouei, P., Kalkhoran, S.B., and Hausenloy, D.J. (2015). The mitochondrial permeability transition pore and its role in myocardial ischemia reperfusion injury. J Mol Cell Cardiol *78*, 23-34.

Panel, M., Ghaleh, B., and Morin, D. (2018). Mitochondria and aging: A role for the mitochondrial transition pore? Aging cell *17*, e12793.
Perez, M.J., Ponce, D.P., Aranguiz, A., Behrens, M.I., and Quintanilla, R.A. (2018). Mitochondrial permeability transition pore contributes to mitochondrial dysfunction in fibroblasts of patients with sporadic Alzheimer's disease. Redox Biol *19*, 290-300.
Rao, K.V., and Norenberg, M.D. (2004). Manganese induces the mitochondrial permeability transition in cultured astrocytes. The Journal of biological chemistry *279*, 32333-32338.
Rea, S.L., Ventura, N., and Johnson, T.E. (2007). Relationship between mitochondrial electron transport chain dysfunction, development, and life extension in Caenorhabditis elegans. PLoS biology *5*, e259.
Rolland, S.G., Schneid, S., Schwarz, M., Rackles, E., Fischer, C., Haeussler, S., Regmi, S.G., Yeroslaviz, A., Habermann, B., Mokranjac, D.*, et al.* (2019). Compromised Mitochondrial Protein Import Acts as a Signal for UPR(mt). Cell Rep *28*, 1659-1669 e1655.
Rottenberg, H., and Hoek, J.B. (2017). The path from mitochondrial ROS to aging runs through the mitochondrial permeability transition pore. Aging cell *16*, 943-955.
Rual, J.F., Ceron, J., Koreth, J., Hao, T., Nicot, A.S., Hirozane-Kishikawa, T., Vandenhaute, J., Orkin, S.H., Hill, D.E., van den Heuvel, S.*, et al.* (2004). Toward improving Caenorhabditis elegans phenome mapping with an ORFeome-based RNAi library. Genome Res *14*, 2162-2168.
Sorrentino, V., Romani, M., Mouchiroud, L., Beck, J.S., Zhang, H., D'Amico, D., Moullan, N., Potenza, F., Schmid, A.W., Rietsch, S.*, et al.* (2017). Enhancing mitochondrial proteostasis reduces amyloid-beta proteotoxicity. Nature *552*, 187-193.
Takahashi, N., Hayano, T., and Suzuki, M. (1989). Peptidyl-prolyl cis-trans isomerase is the cyclosporin A-binding protein cyclophilin. Nature *337*, 473-475.
Tian, Y., Garcia, G., Bian, Q., Steffen, K.K., Joe, L., Wolff, S., Meyer, B.J., and Dillin, A. (2016). Mitochondrial Stress Induces Chromatin Reorganization to Promote Longevity and UPR(mt). Cell *165*, 1197-1208.
Urbani, A., Giorgio, V., Carrer, A., Franchin, C., Arrigoni, G., Jiko, C., Abe, K., Maeda, S., Shinzawa-Itoh, K., Bogers, J.F.M.*, et al.* (2019). Purified F-ATP synthase forms a Ca(2+)-dependent high-conductance channel matching the mitochondrial permeability transition pore. Nat Commun *10*, 4341.
Ye, X., Linton, J.M., Schork, N.J., Buck, L.B., and Petrascheck, M. (2014). A pharmacological network for lifespan extension in Caenorhabditis elegans. Aging cell *13*, 206-215.
Yoneda, T., Benedetti, C., Urano, F., Clark, S.G., Harding, H.P., and Ron, D. (2004). Compartment-specific perturbation of protein handling activates genes encoding mitochondrial chaperones. Journal of cell science *117*, 4055-4066.
Yung, H.W., Colleoni, F., Dommett, E., Cindrova-Davies, T., Kingdom, J., Murray, A.J., and Burton, G.J. (2019). Noncanonical mitochondrial unfolded protein response impairs placental oxidative phosphorylation in early-onset preeclampsia. Proceedings of the National Academy of Sciences of the United States of America *116*, 18109-18118.
Zhang, F., Peng, D., Cheng, C., Zhou, W., Ju, S., Wan, D., Yu, Z., Shi, J., Deng, Y., Wang, F.*, et al.* (2016). Bacillus thuringiensis Crystal Protein Cry6Aa Triggers Caenorhabditis elegans Necrosis Pathway Mediated by Aspartic Protease (ASP-1). PLoS pathogens *12*, e1005389.
Zhang, Q., Wu, X., Chen, P., Liu, L., Xin, N., Tian, Y., and Dillin, A. (2018). The Mitochondrial Unfolded Protein Response Is Mediated Cell-Non-autonomously by Retromer-Dependent Wnt Signaling. Cell *174*, 870-883 e817.

Zheng, J., and Ramirez, V.D. (1999). Purification and identification of an estrogen binding protein from rat brain: oligomycin sensitivity-conferring protein (OSCP), a subunit of mitochondrial F0F1-ATP synthase/ATPase. J Steroid Biochem Mol Biol *68*, 65-75.

SUPPLEMENTAL DATA

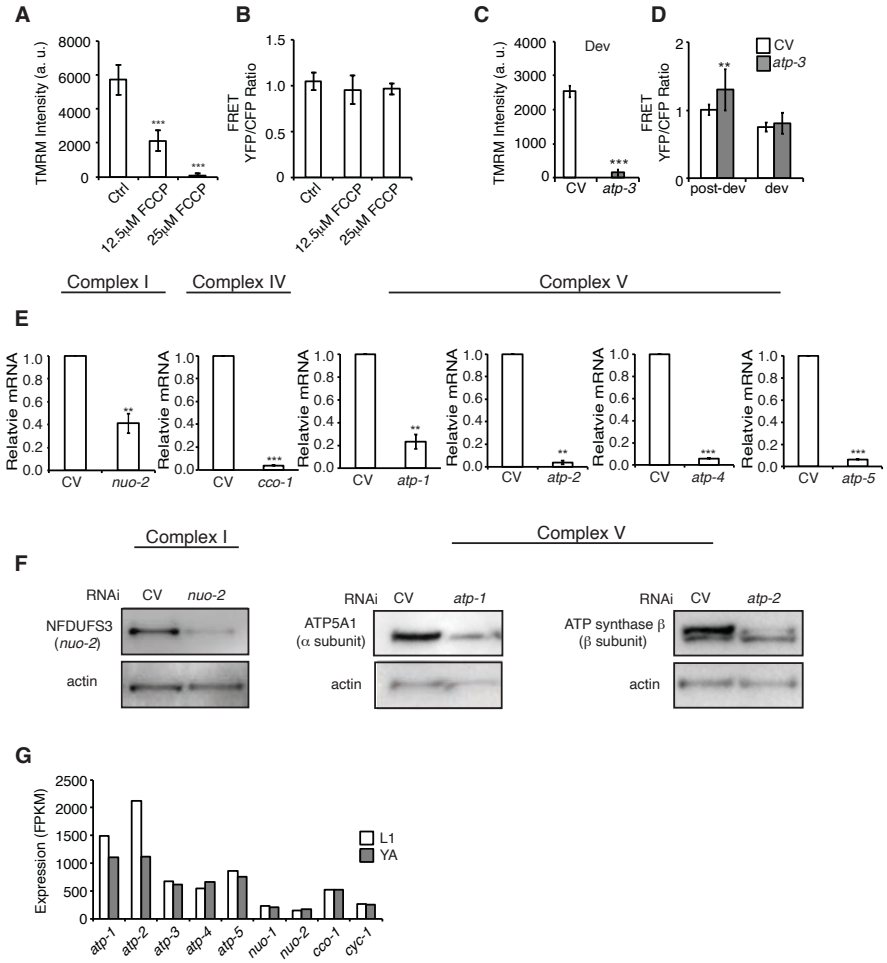

Figure 1- figure supplement 1: RNAi of OSCP/*atp-3* RNAi Uniquely Causes a Loss in Membrane Potential and a Rise in Cytosolic Calcium.

(A) FCCP, the mitochondrial uncoupler, significantly induces a loss in MMP. FCCP was administered for 24- 48 hours beginning at young adulthood. Data are the mean ± SEM of ≤ 15 animals from three biological experiments. ***p ≤ .0001 by Student's *t*-test.

(B) FCCP does not affect significantly alter cytosolic Ca^{2+} using the FRET-based calcium indicator protein D3cpv/cameleon. Data are the mean ± SEM of ≤ 15 animals from three biological experiments.

(C) Developmental RNAi of OSCP/*atp-3* induces a loss in MMP. RNAi was administered beginning from eggs for 72 hours. TMRM was spotted on seeded plates. ***p ≤ .0001 by Student's *t*-test.

(D) Developmental RNAi of OSCP/*atp-3* does not significantly alter cytosolic Ca^{2+} using the FRET-based calcium indicator protein D3cpv/cameleon compared to post-developmental RNAi. Developmental RNAi was administered beginning from eggs for 72 hours. Post-developmental RNAi was administered for 48 hours beginning from young adulthood. **p ≤ .01 by Student's *t*-test.

(E) qPCR from N2 worms after RNAi of subunits from complex I, IV and V. RNAi was administered for 48 hours beginning at young adulthood. Data are the mean ± SD ≤ 150 animals combined from two experiments. **p ≤ 0.01, ***p ≤ .0001 by Student's *t*-test.

(F) Immunoblots from N2 worms after RNAi of subunits from complex I and V. RNAi was administered for 48 hours beginning at young adulthood. Representative immunoblots from two biological experiments. Actin was used as a loading control.

(G) FPKM expression values of various OXPHOS subunits collected at L1 larval stage or young adulthood (YA) from *wormbase.org*.

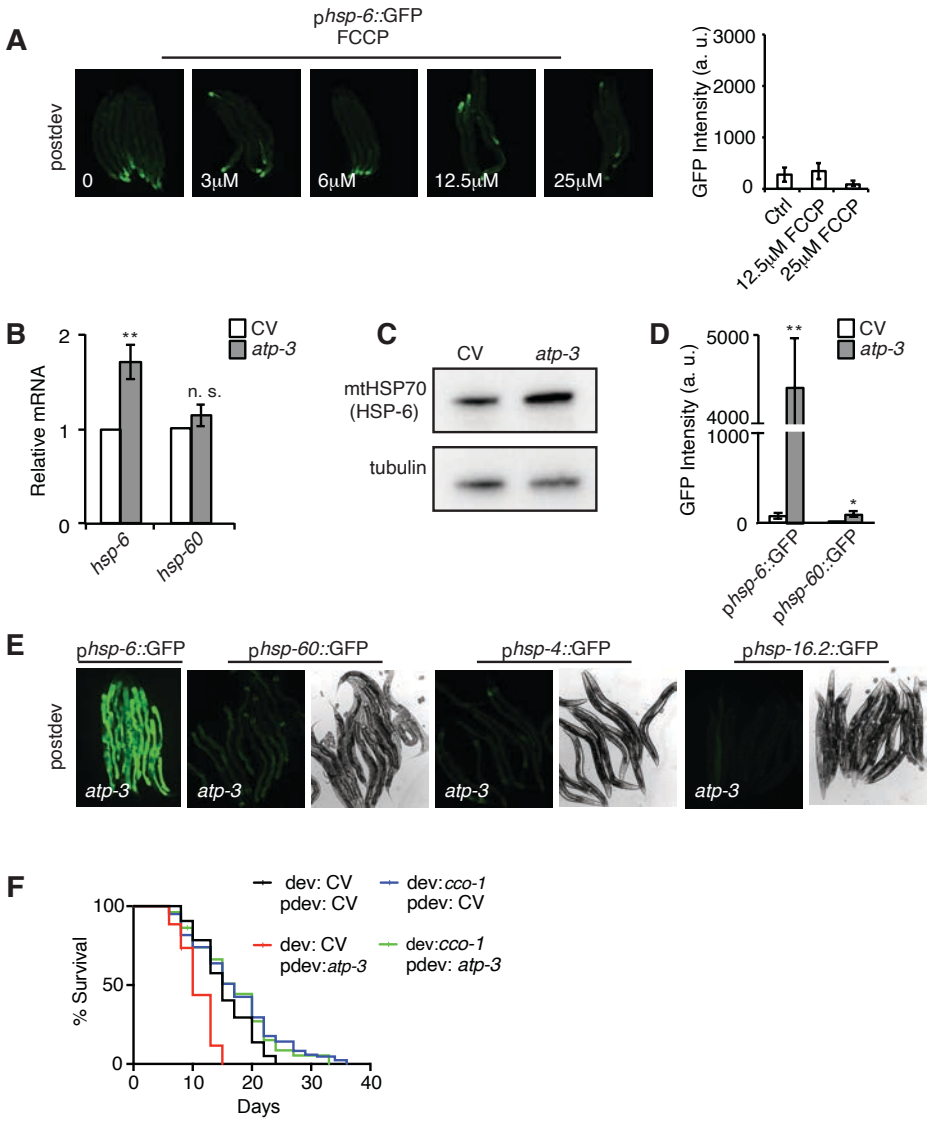

Figure 2- figure supplement 2: Loss of the ATP Synthase Subunit, OSCP/*atp-3*, Induces a Specific, Temporally Confined, and Reversible Post-Developmental UPR^{mt}

(A) Dose response of FCCP, the mitochondrial uncoupler, on the p*hsp-6*::GFP reporter. Quantification of the two highest doses of FCCP from the p*hsp-6*::GFP.

(B) qRTPCR of *hsp-6* and *hsp-60* from N2 worms on post-developmental CV or *atp-3* RNAi. Data are the mean ± SEM of ≤ 150 animals combined from four biological experiments. **p ≤ 0.01, n.s. not significant by Student's *t*-test. CV, control vector RNAi.

(C) Western blot of mtHSP70/HSP-6 and tubulin (loading control) from worms on post-developmental CV or *atp-3* RNAi. CV, control vector RNAi. Representative blot from three biological experiments.

(D) Quantification of p*hsp-6*::GFP and p*hsp-60*::GFP reporters from (E). Data are the mean ± SEM of ≤ 15 animals combined from three biological experiments. **p ≤ 0.01, *p ≤ 0.05 by Student's *t*-test.

(E) Post-developmental RNAi of *atp-3* mildly induced the mitochondrial p*hsp-60*::GFP reporter but not the UPR^{ER} p*hsp-4*::GFP or HSR p*hsp-16.2*::GFP reporters. Left panel, fluorescent channel; right panel, bright-field channel. CV, control vector RNAi.

(F) Survival curves of wild-type N2 treated with or without developmental COX5B/*cco-1* (from eggs until young adulthood) followed by post-developmental treatment with OSCP/*atp-3* (for 48 hours and then transferred to regular NGM plates for the remainder of the lifespan). Lifespan curves from two pooled biological replicates. CV, control vector RNAi; dev, developmental; pdev, post-developmental.

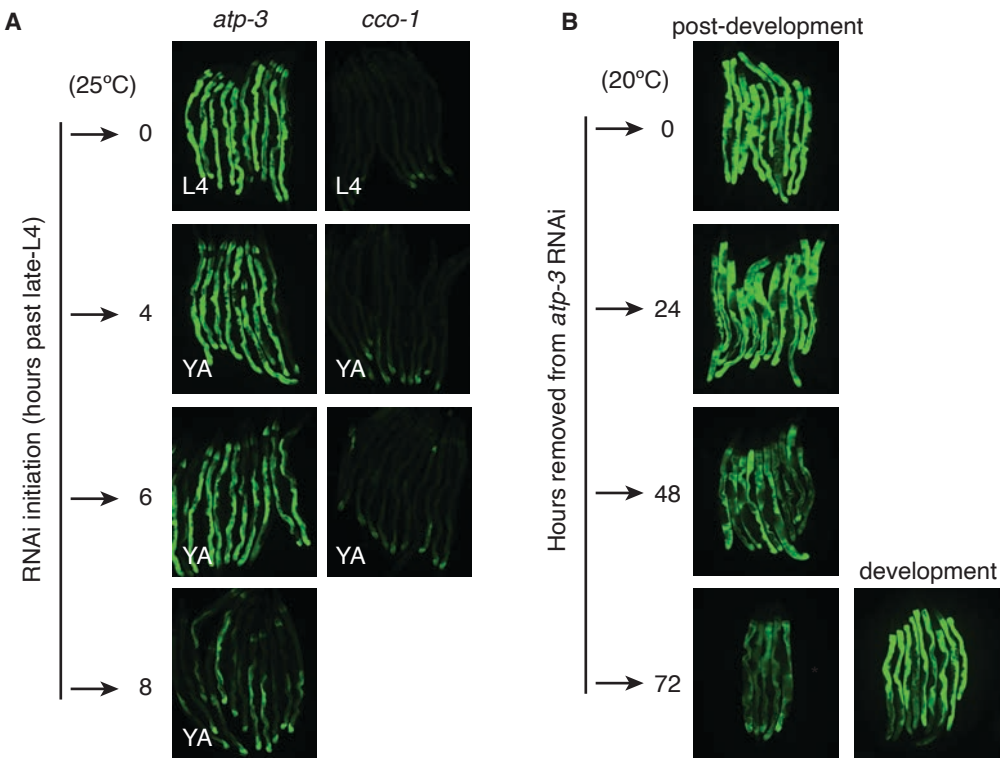

Figure 2- figure supplement 3: The Post-Developmental UPR^{mt} is Temporally Confined and Reversible
(A) Post-developmental RNAi of OSCP/*atp-3* or COX5B/*cco-1* RNAi that was initiated at L4, young adult, and adult stages using the p*hsp-6*::GFP reporter at 25°C. GFP expression was assessed 48 hours after RNAi initiation. Representative pictures from two biological experiments.
(B) The p*hsp-6*::GFP reporter worms were treated with developmental or post-developmental OSCP/*atp-3* RNAi. Worms were removed from HT115 RNAi bacteria and placed onto OP50 bacteria and GFP expression was assessed at indicated time-points. Representative pictures from two biological experiments.

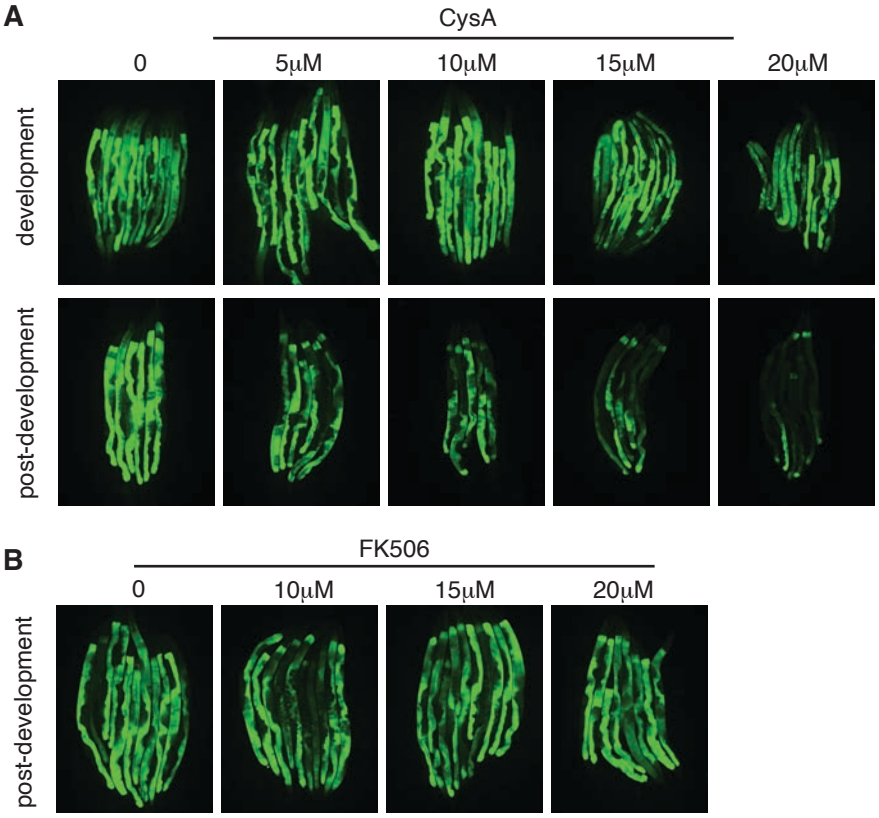

Figure 3- figure supplement 4: Loss of OSCP/*atp-3* in Adulthood Recapitulates mPTP characteristics
(A) Dose response of CsA administered during development or post-development on OSCP/*atp-3* RNAi-treated p*hsp-6*::GFP reporter worms. Developmental RNAi was administered beginning from eggs for 72 hours. Post-developmental RNAi was administered for 48 hours beginning from young adulthood.
(B) Dose response of FK506 administered during post-development on OSCP/*atp-3* RNAi-treated p*hsp-6*::GFP reporter worms. Post-developmental RNAi was administered for 48 hours beginning from young adulthood.

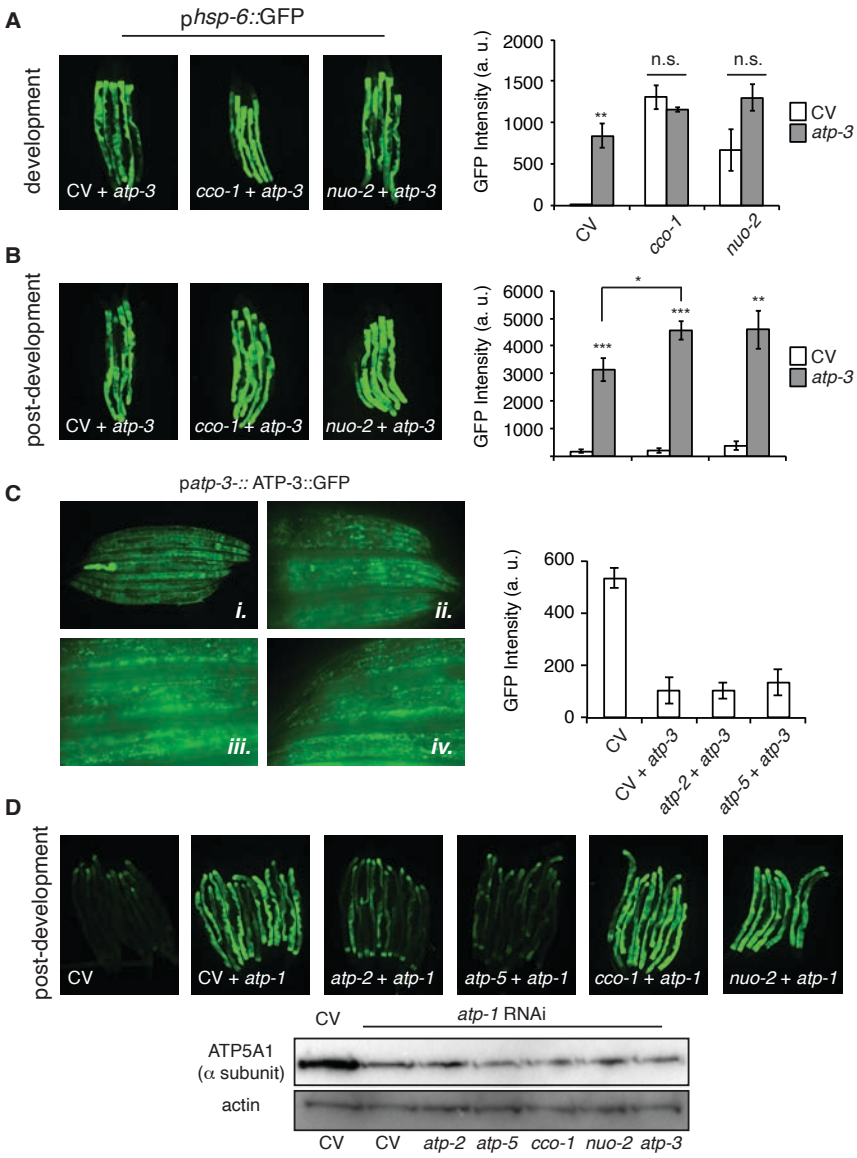

Figure 5 -figure supplement 5: Effects of Loss of OXPHOS Subunits on the dvUPR^{mt} and pdvUPR^{mt}
(A, B) Concomitant developmental (A) or post-developmental (B) RNAi of *atp-3* and either *cco-1* or *nuo-2* induced the p*hsp-6*::GFP reporter. For developmental treatment, worms were exposed to RNAi beginning from eggs for 72 hours. For post-developmental treatment, worms were exposed to RNAi from young adulthood for 48 hours. Bar graphs are the mean ± SEM of ≤ 15 animals combined from three biological experiments. ** p ≤ .0001, ***p ≤ .0001 by Student's *t*-test. n. s., no significant differences from CV + *atp-3* condition; dvUPR^{mt}, development; pdv, post-development; CV, control vector.
(C) Dual-RNAi effectively knocks down ATP-3 protein synthesis as measured by the translational p*atp-3*::ATP-3::GFP reporter, i.10X photomicrographs of homozygous and heterozygous (bright pharyngeal GFP expression) worms, ii. 40X photomicrographs of head region of control homozygous worms, iii. 40X photomicrographs of mid-region of control homozygous worms, iv. 40X photomicrographs of tail region of control homozygous worms.
(D) RNAi of α/*atp-1* induces a post-developmental UPR^{mt} similar to OSCP/*atp-3* in the p*hsp-6*::GFP reporter. Representative results from two biological experiments. Immunoblot of ATP-1 from p*hsp-6*::GFP reporter worms after dual-RNAi treatment for 48 hours. Representative blots from two biological experiments.

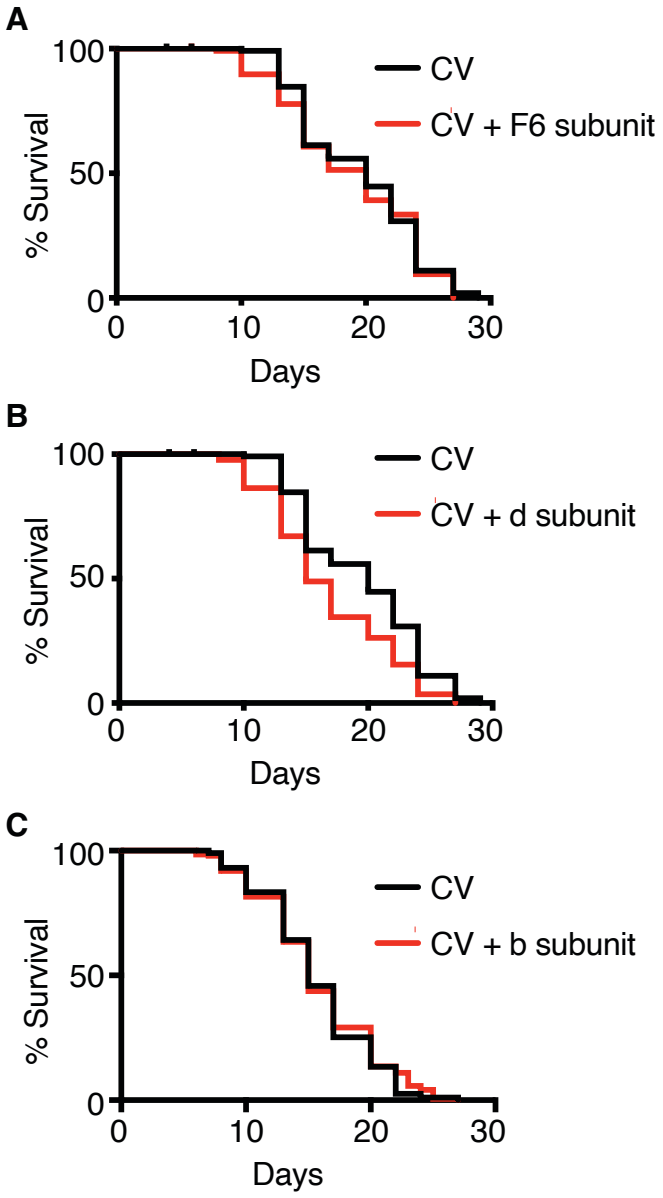

Figure 6- figure supplement 6: Post-Developmental Loss of F-ATP Synthase Peripheral Stalk Subunits
(A-C) Survival curves of wild-type N2 worms on indicated RNAi. RNAi was administered starting from young adulthood for 48 hours and then transferred to regular NGM plates for the remainder of the lifespan. Pooled survival curves from two biological experiments.

SUPPLEMENTAL TABLES

	gene	dvUPR^{mt}	pdvUPR^{mt}	pdvUPR^{mt} fold change	p-value
Complex I	*nuo-1*	yes	yes	2.6	0.0002
	nuo-2	yes	yes	2.1	0.0155
Complex III	*cyc-1*	yes	yes	2.1	< 0.0001
Complex IV	*cco-1*	yes	no	1.9	0.0511
Complex V	*atp-2*	yes	yes	2.7	0.0029
	atp-3	yes	yes	71.6	< 0.0001
Other	*clk-1*	yes	no	-1.5	0.0064
	mrps-5	yes	no	1.0	0.9671
	tomm-22	yes	no	-1.8	0.0004

Figure 2- table supplement 1: List of genes tested for whether they induce a developmental UPR^{mt} (dvUPR^{mt}) or post-developmental UPR^{mt} (pdvUPR^{mt}).

gene	MTS strength
cyn-1	0.941
cyn-2	0.0
cyn-3	0.0
cyn-4	0.0
cyn-5	0.0
cyn-6	0.0
cyn-7	0.0
cyn-8	0.0
cyn-9	0.0
cyn-10	0.0
cyn-11	0.0
cyn-12	0.0
cyn-13	0.0
cyn-14	0.0
cyn-15	0.0
cyn-16	0.0
cyn-17	0.154
atfs-1	0.117

Figure 3- table supplement 2: List of *C. elegans* cyclophilins and their predicted mitochondrial localization using the MitoFates mitochondrial targeting sequence (MTS) prediction tool.

Complex V	gene	subunit	dvUPR^{mt}	pdvUPR^{mt}	pdvUPR^{mt} fold change	p-value
F1 ATPase	*atp-1*	α	yes	yes	19.7	0.0004
F1 ATPase	*atp-2*	β	yes	yes	2.7	0.0029
F1 ATPase	*F58F12.1*	δ	yes	yes	1.5	0.0410
F1 ATPase	*hpo-18*	ε	yes	yes	12.3	< 0.0001
F1 peripheral stalk	*atp-3*	OSCP	yes	yes	55.4	< 0.0001
F1 peripheral stalk	*asb-2*	b	yes	no	1.9	0.0797
F1 peripheral stalk	*atp-5*	d	yes	no	1.1	0.6388
F1 peripheral stalk	*atp-4*	F6	yes	no	1.2	0.2206
Fo rotor	*Y82E9BR.3*	c	yes	yes	3.8	0.0003
Fo supernumerary	*R04F11.2*	e	yes	no	1.0	0.9604
Fo supernumerary	*R53.4*	f	yes	no	1.1	0.7152

Figure 4- table supplement 3: Summary of the effects of RNAi of ATP synthase subunits on the developmental UPR^{mt} (dvUPR^{mt}) or post-developmental UPR^{mt} (pdvUPR^{mt}).

	Strain	Median lifespan (days)	Deaths/Events	Censored Animals	Deaths/Censored	P-value	
Development	N2; CV	15	48	20	48/20		
	N2; atp-3	26.5	34	30	34/30	*** < 0.0001	
	N2; CV	15	161	38	161/38		
Post-development	N2; atp-3	10	181	20	181/20	*** < 0.0001	
	atfs-1; CV	12	117	63	117/63		
	atfs-1; atp-3	9	157	31	157/31	*** < 0.0001	
	N2; CV	17	116	27	116/27		
	N2; cyc-1	17	137	22	137/22	0.6097	
	N2; cco-1	17	139	6	139/6	0.2826	
	N2; atp-2	15	131	22	131/22	** 0.0067	
	N2; nuo-2	17	128	27	128/27	0.5893	
Post-development	N2; CV	15	124	33	124/33		
	N2; atp-3	13	130	16	130/16	*** < 0.0001	
	N2; CV 15uM CysA	17	85	24	85/24		
	N2; atp-3 15uM CysA	17	112	35	112/35	0.6084	
Post-development	N2; CV	15	278	11	278/11		
	N2; atp-1	13	287	13	287/13	** 0.0039	
						Compared to CV	Compared to corresponding RNAi
Post-development	N2; CV	15	199	10	199/10		
	N2; CV/atp-3	13	183	48	183/48	*** < 0.0001	
	N2; CV/asb-2	15	193	4	193/4	0.4473	
	N2; atp-3/asb-2	15	198	6	198/6		0.0811
	N2; CV/Y82E9BR.3	20	135	0	135/0	*** < 0.0001	
	N2; atp-3/Y82E9BR.3	20	129	6	129/6		0.2578
						Compared to CV	Compared to corresponding RNAi
Post-development	N2; CV	20	106	11	106/11		
	N2; CV/atp-3	13	106	10	106/10	*** < 0.0001	
	N2; CV/atp-4	20	110	8	110/8	0.5035	
	N2; atp-3/atp-4	17	108	3	108/3		0.3437
	N2; CV/atp-5	15	86	2	86/2	** 0.0006	
	N2; atp-3/atp-5	20	100	5	100/5		** 0.0036
development; post-development	N2; CV; CV	15	139	0	139/0		
	N2; CV; atp-3	10	138	2	138/2	*** < 0.0001	
	N2; cco-1; CV	17	87	13	87/13	** 0.0031	
	N2; cco-1; atp-3	17	102	30	102/30		0.6294

Source Data 1: Summary of lifespans.